REVIEW

Check for updates

Metal–organic frameworks (MOFs) as apt luminescent probes for the detection of biochemical analytes

Dongwen Luo,[†ab] Jiefeng Huang,[†b] Yanhong Jian,[†b] Ayushi Singh, [iD] [d]
Abhinav Kumar, [iD] *[d] Jianqiang Liu, [iD] *[bde] Ying Pan*[ab] and Qin Ouyang*[c]

The detection of active substances in the body is very important for good human health as it gives important insights into the smooth functioning of the body. Most of the conventional materials that can be used as suitable probes require complicated fabrication methodologies, have poor stability and are susceptible to environmental effects. In contrast, metal–organic frameworks (MOFs) offer unique advantages as probes for testing analytes due to their tunable porosity, good specific surface area and ease of modification. Unlike previously reported perspectives/reviews, this perspective focuses on the latest applications of MOFs as detection materials for hydrogen peroxide, various metal ions, hydrogen sulfide, organic small molecules, glutathione, and organic macromolecules such as nucleic acids, and focuses on providing a more detailed mechanism of action. Also, the basic principles of action utilized by this class of materials are discussed.

1. Introduction

There are many physiologically active substances in human cells, *viz.* hydrogen peroxide, hydrogen sulfide, various classes of organic molecules and ions and others. These biologically active substances play a very important role in the normal physiological functioning of cells. They are responsible for a wide range of functions such as bio-catalysis, regulation and information transfer in various metabolisms and contribute to various cellular processes such as differentiation, growth, migration, proliferation and phagocytosis. These phenomena play a vital role in the maintenance of the body's optimal state and hence, detection of these cellular components is essential to understand the biochemical phenomenon appropriately. Also, the accurate detection of these active substances develops a deep understanding of the current state of cellular health, health screening and the diagnosis as well as the treatment of

diseases. However, testing of these active substances requires the use of specialized materials.

Over the past few decades, investigators have developed a range of materials for the detection of these active substances that are broadly categorized as natural enzyme-based detection materials, enzyme-like bioactive detection materials and non-enzyme detection materials. Natural enzyme-based detection materials have some inherent disadvantages, including their inherent instability, vulnerability to external influences, susceptibility to deactivation, and stringent experimental requirements.[1] Enzyme-like detection materials include conducting polymers, metals and their compounds, mesoporous carbon and graphene composites, among others.[2] These materials are highly sensitive and are currently used in the detection of various analytes; while non-enzymatic detection materials include noble metals,[3] transition metals,[4] metal oxides,[5] or sulfides,[6] and carbon-based materials.[7] Due to their simplicity, low price, and comparatively high stability, these materials are frequently extensively used. Furthermore, the ability of these materials to combine with certain organic nanoparticles is another crucial quality. Nanomaterials' distinctive physicochemical characteristics, such as their high biocompatibility and outstanding electrical conductivity, enable them to significantly improve the performance of traditional detection materials.

A new class of porous materials known as metal–organic frameworks (MOFs) is made up of coordination bonds that bind metal centers or clusters to organic building blocks.[8,9] MOFs offer benefits such as adjustable porosity, high specific surface area, and customizable architectures when compared to

[a] *The First Dongguan Affiliated Hospital, Guangdong Medical University, Dongguan, 523808, China. E-mail: panying@gdmu.edu.cn*

[b] *Guangdong Provincial Key Laboratory of Research and Development of Natural Drugs, and School of Pharmacy, Guangdong Medical University, Guangdong Medical University Key Laboratory of Research and Development of New Medical Materials, Dongguan, 523808, China. E-mail: jianqiangliu2010@126.com*

[c] *Department of General Surgery, Dalang Hospital, Dongguan, Guangdong, China. E-mail: ouyangqin8@sina.com*

[d] *Department of Chemistry, Faculty of Science, University of Lucknow, Lucknow-226007, India. E-mail: abhinavmarshal@gmail.com*

[e] *Affiliated Hospital of Guangdong Medical University, Zhanjiang, Guangdong, China*

† These authors contributed equally to this work.

typical porous materials such as porous carbon, porous catalysts and porous polymers.[10–14] All these properties could (at least theoretically) address the need to develop novel sensing materials with high sensitivity, excellent selectivity, fast response times, enhanced stability and reusability.[15] Hence, MOF materials have promising future in the fields of bioimaging, adsorption,[16,17] catalysis,[18] magnetism,[19] sensing,[20,21] and drug delivery.[22] Recently, the biological uses of MOFs have drawn a lot of attention in recent years, particularly in the area of electrochemical biosensing.[15,23,24] MOFs possess open metal sites at their backbone that provide mimetic catalytic properties and amplify electrochemical signals that effectively improve the sensitivity of detection.[25] Recently, researchers have employed MOFs as biosensors for the detection of different components in cells such as deoxyribonucleic acid (DNA), ribonucleic acid (RNA), glutathione (GSH),[26] metal ions,[27–29] and cancer biomarkers (hydrogen sulfide (H_2S), hydrogen peroxide (H_2O_2), and ascorbic acid).[30–32] Also, as compared to conventional detection techniques, MOF-based biosensors have better sensing efficiency, enabling detection at fg mL^{-1} or even lower concentrations.[33,34]

The basic principle of MOF-based materials for sensing of analytes is shown in Fig. 1. The mechanism of action mainly involves the following steps: first, the material catalyzes the reduction of the analytes to produce an electrochemical signal; second, the structure of the material is altered upon interaction with the analyte, thus producing a fluorescent effect; third, certain materials have a fluorescent effect of their own and undergo a fluorescence enhancement on interaction with the analytes. Since different analytes have to be detected, the materials used for the detection these analytes are also different. The timeline for the development of MOFs for the detection of glutathione, hydrogen peroxide, hydrogen sulfide and ionophores is presented in Fig. 2.

In view of the importance of MOFs as apt sensing systems to selectively and efficiently detect a plethora of biological analytes, this perspective focuses on the recent investigations on the use of MOFs as biosensors for the detection of hydrogen peroxide (H_2O_2), metal ions, hydrogen sulfide and organic molecules in biological cells. The main MOF-based materials as sensors for the analytes mentioned in this paper are classified and presented in Table 1.
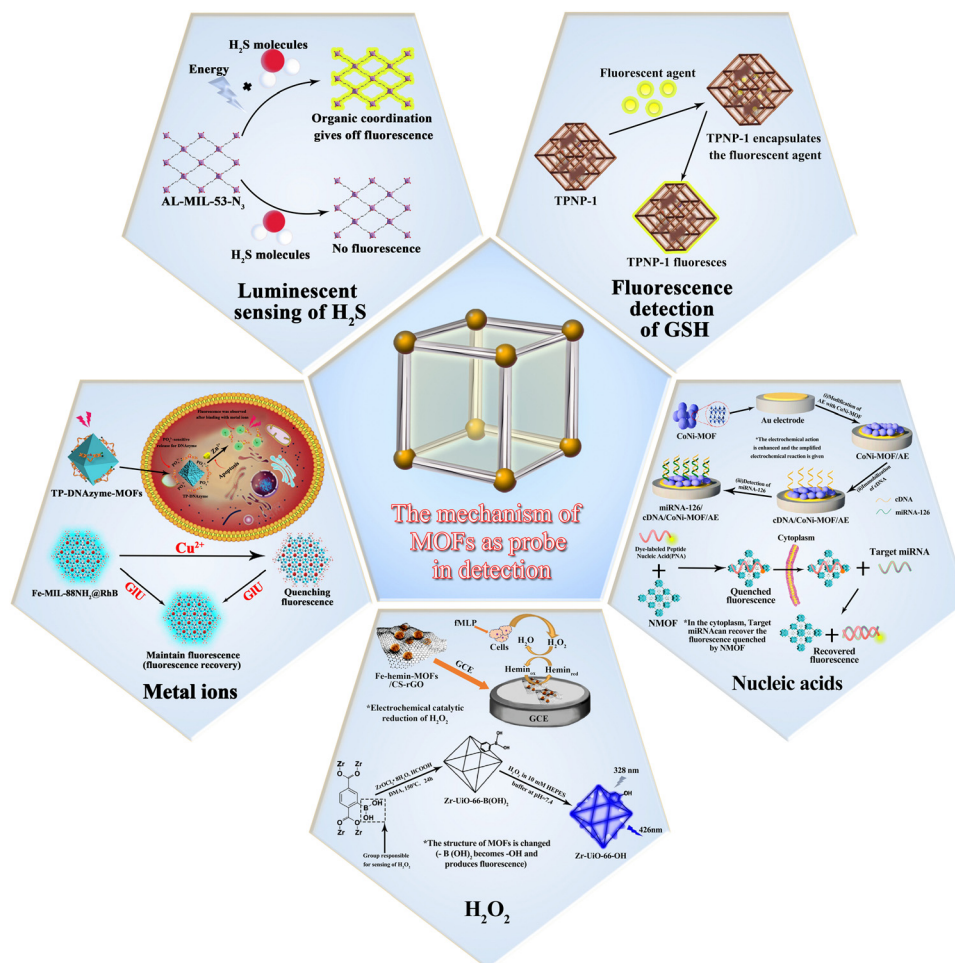

Fig. 1 The basic principles utilized for sensing of biochemical analytes by MOF-based materials.

This journal is © The Royal Society of Chemistry 2023

J. Mater. Chem. B, 2023, **11**, 6802–6822 | **6803**

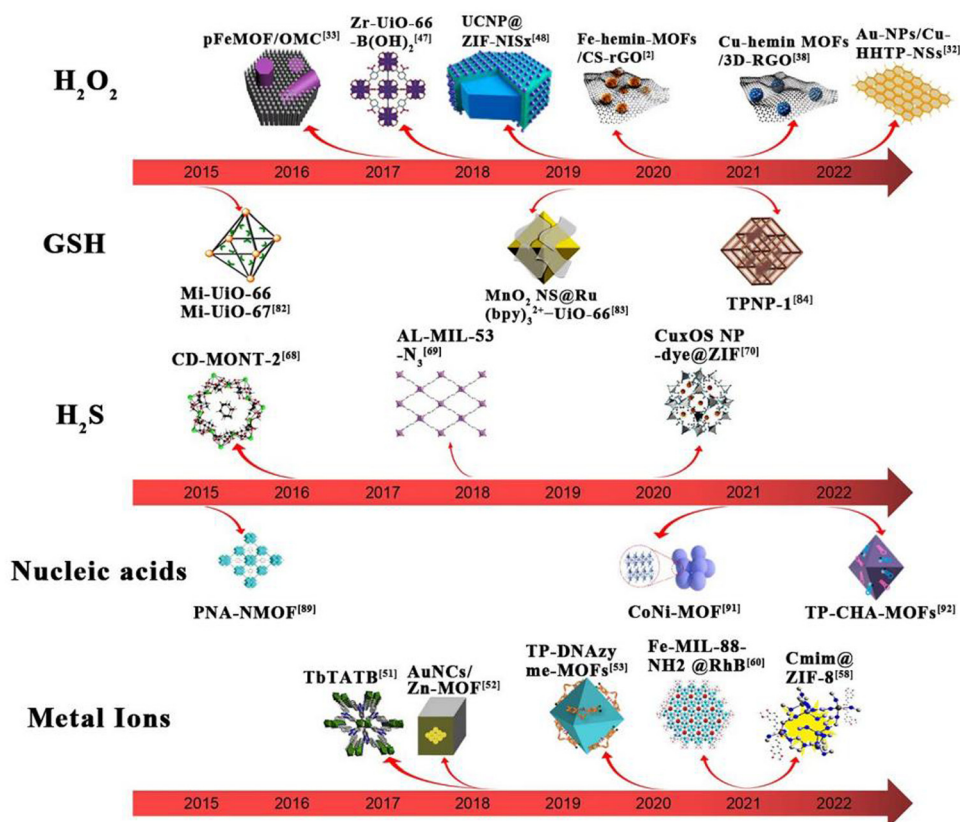Fig. 2 Timeline for the development of tests for MOFs in five areas.

Table 1 MOF-based materials as sensors for different biochemical analytes

MOF	Substances tested	Synthetic method	Detection limits	Detection range	Ref.
Fe-Hemin-MOFs	H_2O_2	Ultrasound synthesis method	0.57 μM	1–61 μM, 61–1311 μM	2
Au-NPs/Cu-HHTP-NSs	H_2O_2	Solvothermal method	0.0056 μM	50 nM–16.4 mM	46
pFeMOF/OMC	H_2O_2	Hydrothermal method	0.45 μM	0.5–70.5 μM, 70.5–1830.5 μM	47
AuNFs/Fe$_3$O$_4$@ZIF-8-MoS$_2$	H_2O_2	Electrochemical deposition method	0.9 μM	5 μM–120 mM	48
ZIF-67-Au@Pt	H_2O_2	Ultrasound synthesis method	0.086 μM	0.8 μM–3 mM	49
SGO@HKUST-1	H_2O_2	Solvothermal method	0.49 μM	1 μM–5.6 mM	50
PtCu@MOF/C	H_2O_2	Self-sacrificing templates	0.22 μM	1 μM–3 mM	51
Cu-Hemin MOFs/3D-RGO	H_2O_2	Co-precipitation method	0.14 μM	10–24400 μM	52
MIL-47(V)-OH	H_2O_2	Electrochemical methods	4.38 μM	4.38–43.98 μM, 50.33 μM–2.24 mM	53
Zr-UiO-66-B(OH)$_2$	H_2O_2	Solvothermal method	0.015 μM	—	60
UCNP@ZIF-NiSx	H_2O_2	*In situ* growth method	0.032 μM	0.05–20 μM	61
TbTATB	Zn^{2+}	Solvothermal method	0.0105 μM	—	64
AuNCs/Zn-MOF	Zn^{2+}	Hydrothermal method	0.006 μM	12.3 nM–24.6 mM	65
DNAzyme-MOFs	Zn^{2+}	DNA solid phase synthesis, solvothermal method	0.0035 μM	—	66
ZIF-8@Cmim	Fe^{2+}	Solvothermal method	7.64 μM	—	71
Fe-MIL-88NH$_2$@RhB	Cu^{2+}	Solvothermal method	4.23 μM	—	73
UiO-66@N$_3$	H_2S	Solvothermal method	118 μM	—	80
CD-MONT-2	H_2S	Solvothermal method	0.058 μM	—	81
Al-MIL-53-N$_3$	H_2S	Solvothermal method	0.090 μM	—	82
CuxOS-@ZIF-8	H_2S	*In situ* growth method	0.0022 μM	—	83
Mi-UiO-67	GSH	Solvothermal method	0.010 μM	—	95
MnO$_2$ NS@Ru(bpy)$_3$$^{2+}$-UiO-66	GSH	*In situ* growth method	0.28 μM	—	96
TPNP-1	GSH	Solvothermal method	0.087 μM	0–80 μM	97
PANMOF	miRNA	*In situ* growth method	∼0.001 μM	0–1000 nM	102
CoNi-MOF	miRNA	Solvothermal method	0.0014 μM	1–10 nM	104
TP-CHA-UiO-66	miRNA	Solvothermal method	160 μM	1–60 nM	105

2. Application of MOFs in the detection of H$_2$O$_2$

2.1. Electrochemical detection method

As one of the body's metabolites and a key mediator in physiological processes, hydrogen peroxide (H$_2$O$_2$), a reactive oxygen species (ROS) produced by the respiratory chain and cellular metabolism, plays a critical role in cell proliferation, cell differentiation, cell death, intracellular signaling, mediating immune responses and chronic disease responses. It majorly contributes towards the oxidative stress in the organism.[35,36] Excess H$_2$O$_2$ can cause cytotoxicity and cellular damage by attacking methionine residues and cysteines. On the other hand, its high content can also lead to some pathological defects, such as cancer,[37,38] diabetes,[39,40] Alzheimer's disease,[41,42] nucleic acid damage,[43] and so on. Since H$_2$O$_2$ is closely linked to signal transduction and cellular activity, sensitive monitoring and effective regulation of intracellular H$_2$O$_2$ levels is therefore essential in health screening, disease diagnosis and therapy. The ordered structural framework of MOFs can lead to specific reactions that can be repeatedly used for the detection of specific analytes due to their stability.[34] However, accurate and sensitive detection of intracellular H$_2$O$_2$ is not an easy task due to the complex and variable nature of the cellular environment. Although scientists have developed several analytical strategies, including photoelectrochemical, fluorescence and spectrophotometric methods, to detect H$_2$O$_2$, these methods have limitations due to the requirements of expensive fluorescent agents, complex operational procedures and low sensitivity. In contrast to these approaches, electrochemical biosensors have gained attention because of their high sensitivity, quick analysis, and real-time on-line continuous monitoring in complex systems.[44] Because of their great sensitivity and specificity, natural enzymes were commonly utilized in the early days of electrochemical H$_2$O$_2$ sensors.[45] However, their utilities as sensors were constrained by the enzyme's inherent disadvantages. MOFs ameliorate the inherent shortcomings of these enzymes when paired with them due to their unique qualities (e.g., structural porosity and functional variety).

A new heme metal–organic framework (Fe-hemin-MOFs) with distinct peroxidase-like bioactivity was reported by Zhao et al. This material exhibited excellent hydrogen peroxide catalytic activity and can be further loaded with chitosan-reduced graphene oxide (CS-rGO), which resulted in an enhanced electrochemical signal. The mechanism of action is as follows: H$_2$O$_2$ is first reduced to H$_2$O via the material catalytic center hemin (Fe^{2+}), which is oxidized to hemin (Fe^{3+}). Hemin (Fe^{3+}) is then reduced at the electrode and generates an electrical signal. In this process, CS-rGO accelerates the transfer of electrons and further promotes the catalytic process of H$_2$O$_2$. The ligand structure of the haemoglobin-MOFs can shield the haemoglobin active centre and increases stability, and haemoglobin can imitate artificial enzymes with strong electrocatalytic activity. The synergistic effect of CS-rGO and Fe-hemin-MOFs could have an enhanced electrochemical signal and provided an excellent H$_2$O$_2$ reduction capability in the sensor. This material had a

lower detection limit than most electrochemical sensors based on peroxidase-like MOFs. This is encouraging for the detection of H$_2$O$_2$ at low concentrations. It also allowed real-time monitoring of H$_2$O$_2$ release from living cells, thereby providing a promising strategy for biomolecular monitoring.[2]

In 2022, Huang and co-workers developed a high-performance electrochemical biosensor based on a highly active dual-nanosome amplification system, comprised of ultrathin two-dimensional (2D) conductive metal–organic framework (C-MOF) nanosheets (NSs) that was modified with high-density ultra-fine gold nanoparticles (Au-NPs), Au-NPs/Cu-HHTP-NSs, and explored its application in the C-MOF-NSs (i.e. Cu-HHTP (HHTP = 2,3,6,7,10,11-hexahydroxybenzophenanthrene)-NSs). These materials provided a large surface area and abundant active open metal sites that greatly enhanced the catalytic activity towards H$_2$O$_2$. The large number of exposed oxygen atoms was used as anchor sites to deposit high density ultrafine Au-NPs without agglomeration (Fig. 3). The material was synthesized using a solvothermal method. The anionic surfactant sodium dodecyl sulphate (SDS) acted as a barrier, reducing interlayer build-up and weakening interlayer interactions, which in-turn resulted in the formation of ultra-thin large size nanosheets during sonication, thereby providing a high specific surface area with abundant anchoring sites. The nanoenzyme Au-NP materials were grown in situ on the reduced precursor tetrachloroauric acid (HAuCl$_4$) without adding reducing or capping agents. Notably, due to the synergistic effect of the highly active Cu-HHTP-NSs and Au-NPs and their unique structural and electrical properties, the prepared nano-hybrid modified electrodes exhibited good sensing performance for H$_2$O$_2$ with extremely low detection limits and high sensitivity.[46]

Also, some enzyme-like materials in combination with MOFs can engender detection materials that display good sensing and detection activity with high accuracy. pFeMOF/OMC, a new porphyrin-iron metal–organic framework (pFeMOF) modified with ordered mesoporous carbon (OMC), was synthesized by Liu et al. in 2017. The mechanism of action of this sensor operated through the reduction of H$_2$O$_2$, generating an electrical signal for detection purposes. Fe^{3+} can strongly coordinate with the carboxylate of the porphyrin moiety to produce an amplified electrochemical signal due to the peroxidase-mimicking properties of pFeMOF. The carbon skeleton of OMC exhibited a limiting effect on the growth of pFeMOF crystals, reducing the aggregation of pFeMOF and thus producing more active sites for H$_2$O$_2$ reduction. Also, an increase in the number of mesopores accelerated the diffusion rate. Additionally, the introduction of OMC improved the conductivity and stability. More importantly, the biosensor possesses the potential to detect the release of H$_2$O$_2$ from living cells and can accurately detect H$_2$O$_2$ even at low concentrations.[47] Lu et al. also developed an electrochemical biosensor Fe$_3$O$_4$@ZIF-8 hybrid nanosensor. This nanosensor was prepared by electrodepositing gold nano-flowers (AuNFs/Fe$_3$O$_4$@ZIF-8-MoS$_2$) on a magnetic metal–organic framework (MMOF) supported over molybdenum disulphide (MoS$_2$) nanosheets in which the magnetic Fe$_3$O$_4$ nanoparticles have high simulated peroxidase activity, while the MOF backbone ZIF-8 possesses a large pore size and high specific surface area.
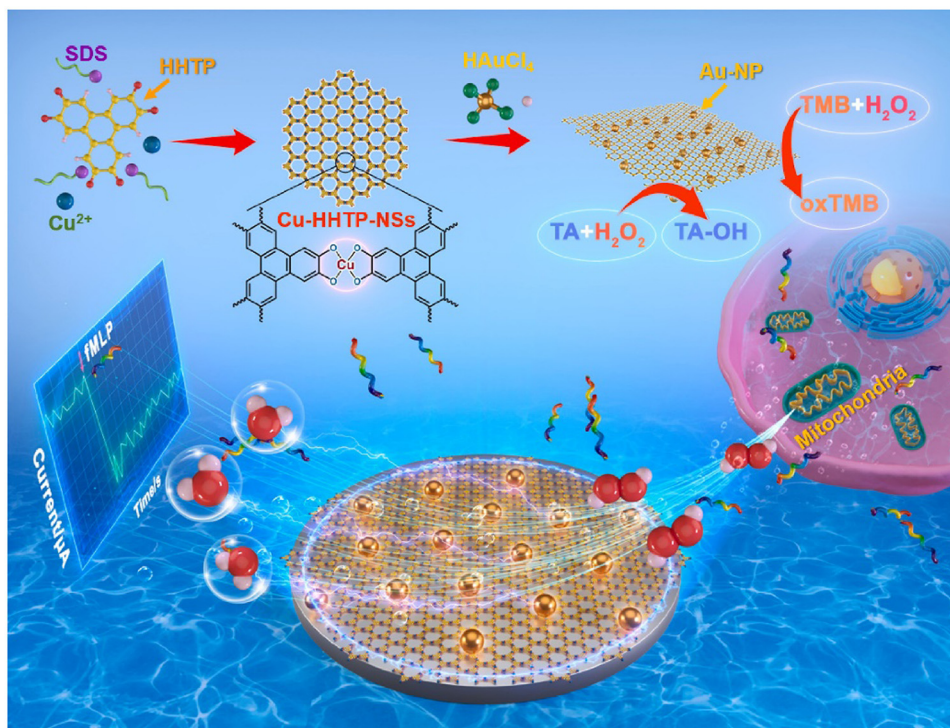
This journal is © The Royal Society of Chemistry 2023

J. Mater. Chem. B, 2023, 11, 6802–6822 | 6805

Fig. 3 Synthesis of Cu-HHTP-NSs and real-time tracking of mitochondrial release of H_2O_2.[46] Reproduced with permission. Copyright 2022, Elsevier.

The mechanism of action of the sensor is as follows: the H_2O_2 released by the cell is specifically captured by it, and the H_2O_2 is reduced by redox reaction and generates an electron transfer effect, thereby producing a characteristic electrical signal. However, it was found that the MMOF Fe_3O_4@ZIF-8 nanomaterials readily dissolved into the electrolyte solution and subsequently generated irreducible electrochemical reactions. Long-term stability, electrical conductivity, and catalytic characteristics of the materials may all be significantly enhanced by MoS_2 nanosheets and one-step electrodeposited gold nanostructures. MoS_2 nanosheets and electrodeposited gold thin films have a considerable impact on the surface state retention of Fe_3O_4@ZIF-8 nanomaterials, as well as their electrocatalytic activity. With a low detection limit of 0.9 μM and an ultra-wide linear range of 5 μM–120 mM, the material demonstrated substantial electrocatalytic reduction activity towards hydrogen peroxide. The sensor has been successfully utilized to track the release of extracellular H_2O_2 from H9C2 cardiomyocytes.

As shown in Fig. 4, H9C2 cardiomyocytes were used as a model for H_2O_2 release from live cells by adding ascorbic acid (AA) as the stimulant and the ability of the sensor to detect H_2O_2 was assessed by detecting superoxide production by dehydrogenation staining (DHE). As shown in Fig. 4A and B, AA-treated H9C2 cells exhibited much higher levels of reactive oxygen species than untreated H9C2 cells. As presented in Fig. 4C, the addition of 400 μM of AA to a PBS solution containing H9C2 cardiomyocytes (2×10^6 cells) resulted in a change in the electrochemical signal of approximately 0.12 μM. There was no significant difference in the current signal with merely AA or cells, demonstrating that H_2O_2 was released by

H9C2 cells. Fig. 4D shows the electrochemical experiments after seeding on cells in culture dishes for phase comparison. Most of the cells were alive and typically attached to the culture dish. However, the sensor posed new challenges in terms of sensitivity and selectivity when it comes to detecting extracellular H_2O_2 in the culture dish. Hence, combining microfluidic chips and electrochemical sensors may give new possibilities for cell attachment and growth in the future, allowing for sensitive and selective observation of cell activity.[48]

Wang *et al.* reported a novel nanosensor for enzymes, ZIF-67-Au@Pt. The nanoparticle ZIF-67 possessed a hollow structure with Au@Pt nano-flowers loaded on its surface. Using the porous nature and large surface area of the MOF material, more particles can be adsorbed for catalysis. The Au@Pt nanoflower structure has a core–shell bimetallic structure. On the surface of the bimetallic catalyst, the Au particles are positively charged, while the addition of a negatively charged second active metal (*e.g.* Pt) increases the negatively charged area of the entire catalyst surface, which facilitated the H_2O_2 catalytic reaction. The sensor had a good linear range of 0.8 μM–3 mM with a correlation coefficient of 0.9936 and a detection limit of 86 nM. The main advantage of this material was that it not only had good electrical conductivity to amplify the current signal, but the core–shell nanoflower formed by Au@Pt can effectively catalyze the oxidation of H_2O_2. This sensor offers a promising application in biomedical monitoring.[49]

In non-enzymatic materials, precise detection of H_2O_2 can be achieved even in the absence of enzyme recognition and catalysis due to the material's inherent activity towards H_2O_2. Wang *et al.* used graphene oxide (GO), benzene 1,3,5-tricarboxylic
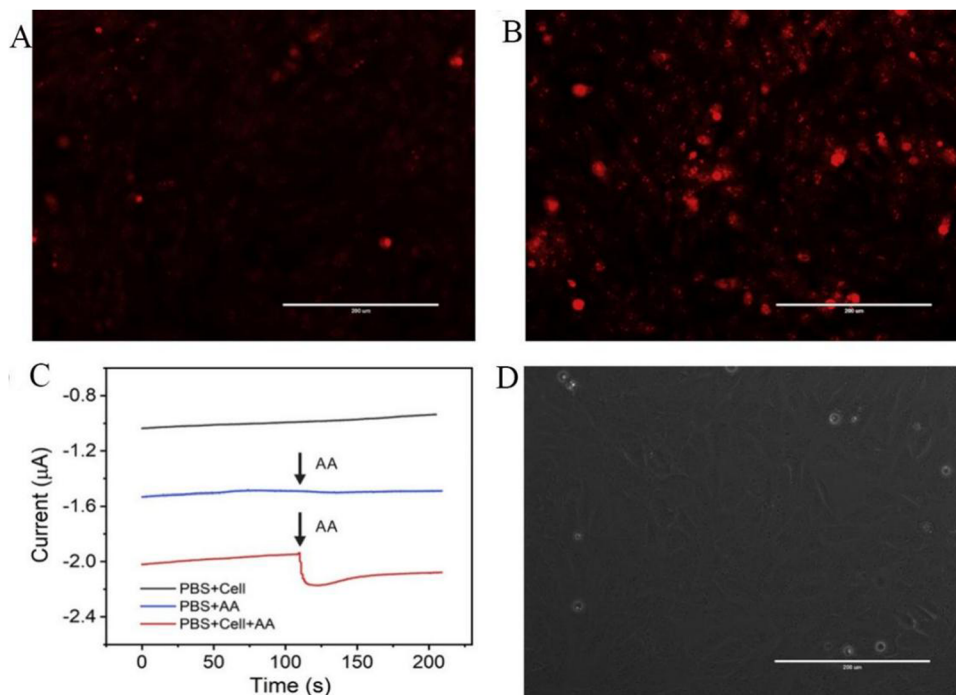
Fig. 4 DHE fluorescence staining of H9C2 cells. (A) Without AA and (B) with 400 μM AA for 5 min. (C) Current effects of AuNFs/Fe₃O₄@ZIF–8–MoS₂/GCE on H9C2 cells spiked with 400 μM AA (with and without H9C2 cells) and H9C2 cells without AA (cell number 2×10^6 cells). (D) Microscopic image of H9C2 cells cultured on a cell culture dish after electrochemical detection (scale bar is 200 μm).[48] Reproduced with permission. Copyright 2020, Elsevier.

acid (BTC) and copper nitrate ($Cu(NO_3)_2$) to synthesize a novel metal–organic backbone (MOF) containing an electroactive nanocomposite with graphene fragments and HKUST-1 to create SGO@HKUST-1. They showed that GO acted as an effective structural guide to induce the transformation of HKUST-1 from an octahedral structure to a hierarchical flower-like structure. The special feature of this process is that the graphene oxide is broken down into small fragments involved in the formation of HKUST-1, which are then converted to their reduced form during the reaction, thereby significantly increasing the surface area, electronic conductivity and redox capacity of the material. In addition, the synergistic interaction of graphene and HKUST-1 provided enhanced electrocatalytic activity, fast responsiveness and high selectivity for H_2O_2 reduction. Compared to other sensors, this sensor showed excellent performance in terms of linear range and detection limits for measuring H_2O_2. The reasons for this may be as follows: first, the presence of abundant and appropriately sized pores of MOFs in the material facilitates the transport of H_2O_2 molecules through the interface; second, the SGO attached to the MOFs has excellent electronic conductivity and high catalytic capacity for the electro-reduction of H_2O_2. This material exhibited satisfactory results as a sensing material for the electrochemical detection of H_2O_2 in complex biological samples (*e.g.* human serum).[50] Chen *et al.* synthesized a unique non-enzymatic electrochemical sensor, PtCu@MOF/C, in which Pt-Cu alloy nanoparticles acted like a H_2O_2 active center that were pre-loaded on a conductive support and wrapped by a copper-based MOF shell using a self-sacrificing template route that formed a semi-enveloped structure. This semi-enclosed structure offered a lower

limit of material detection than the fully enclosed structure of the composite. The synergistic effect operating at the interface between the MOF shell and PtCu conductive support provided better selectivity for the detection of H_2O_2 compared to the unmodified sensor. The novel MOF armored structure of the as-prepared PtCu@MOF/C sensor, especially PtCu@HKUST-1/C with smaller MOF pores, exhibited excellent interference immunity, high stability and high reproducibility in the detection of H_2O_2 (even when released from living cells).[51] Zhou *et al.* in the year 2021 reported a copper-hemin metal–organic framework nano-flower/3D-reduced graphene oxide (Cu-hemin MOFs/3D-RGO) based on copper-hemin MOFs. This nanocomposite material was synthesized by co-precipitation using hemin as a ligand and then modified with 3D-RGO. This nanocomposite exhibited a three-dimensional hollow spherical flower-like structure with large specific surface area and mesoporous properties. This opened up the new possibility of loading more biomolecules and greatly improved the stability by protecting hemoglobin. In addition, the introduction of 3D-RGO effectively enhanced the electrical conductivity of Cu-hemin MOFs, thereby exhibiting good electrochemical properties towards H_2O_2 and enabled *in situ* real-time detection of H_2O_2 release from living cells.[52] Yang *et al.* designed a sensitive sensor, MIL-47(V)-OH, in the presence of negatively charged superoxide ions, that selectively and sensitively detected H_2O_2. Interestingly, by adjusting the ligand in particular by replacing 2-amino terephthalic acid with the 2,5-dihydroxy terephthalic acid of MIL-47(V), the reaction was accelerated at least by a factor of 10 times. In addition, the low detection limit and wide linear range of the MIL-47(V)-OH
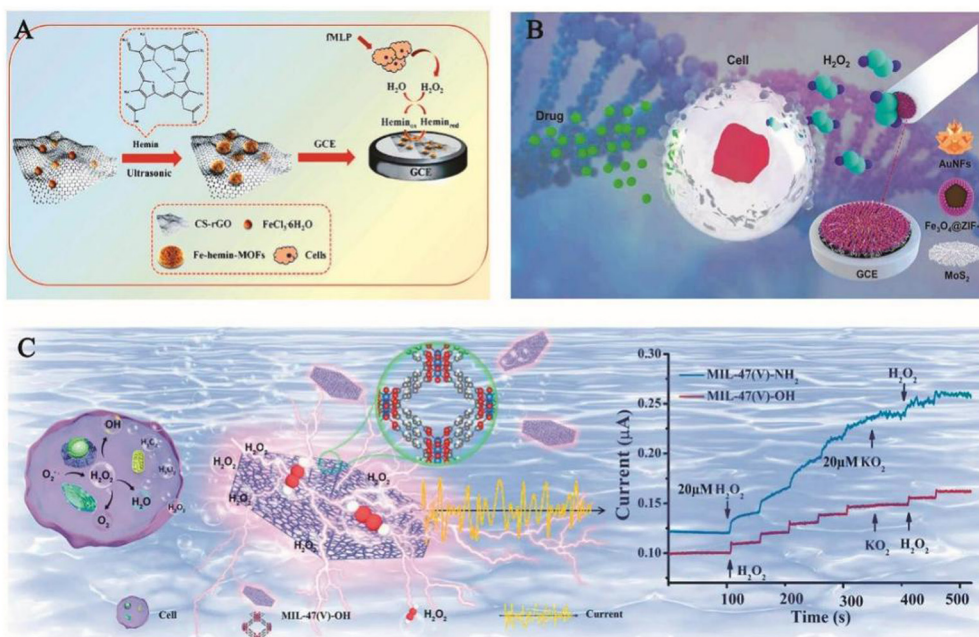
This journal is © The Royal Society of Chemistry 2023

J. Mater. Chem. B, 2023, **11**, 6802–6822 | **6807**

Fig. 5 (A) Schematic diagram of the synthesis of ferrohemoglobin MOFs/CS rGO for real-time monitoring of H_2O_2 released from living cells.[2] Reproduced with permission. Copyright 2020, *Analytica Chimica Acta*. (B) Schematic diagram of an AuNFs/Fe$_3$O$_4$@ZIF-8-MoS$_2$ nanocomposite modified glassy carbon electrode (GCE) for electrochemical determination of H_2O_2 released from living cells under drug stimulation.[48] Reproduced with permission. Copyright 2020, *Sensors and Actuators B: Chemical*. (C) Demonstration of MIL-47(V)-OH (left) detection of H_2O_2 released from tumour cells and rapid detection of H_2O_2 by modulating the ligand of MIL-47 (right).[53] Reproduced with permission. Copyright 2022, Elsevier.

biosensor enabled it to be used for *in situ* monitoring of H_2O_2 release from tumour cells. Also, the conversion of H_2O_2 into superoxide negative ions without applying voltage demonstrated the inhibitory effect of MIL-47 on tumour cells, enabling highly selective and rapid *in situ* detection of H_2O_2 release from living cells.[53]

Of the abovementioned materials, different MOFs showed high sensitivity and accurate detection of hydrogen peroxide *in vivo* due to their unique structural characteristics as electrochemical sensors. The enzyme-like MOFs offered good electrocatalytic effects on hydrogen peroxide artificial enzymes, and the addition of MOFs allowed them to overcome the inherent drawbacks of enzymes, which uplifted their performance. The enzyme-like MOFs can mimic hydrogen peroxide properties and generate amplified electrochemical signals; while for the non-enzymatic MOFs, the synergistic interaction between the components is also active against hydrogen peroxide and they possess high electrical conductivity. In conclusion, these MOF-based materials are important for the detection of hydrogen peroxide *in vivo*. Fig. 5 illustrates the syntheses and application of several representative materials.

2.2. Fluorescence detection method

Among many methods for the detection of hydrogen peroxide *in vivo*, the use of fluorescence spectroscopy employing small molecules has received significant attention. Fluorescence and *in vivo* bioluminescence methods have now been shown to be highly sensitive and selective in the detection of H_2O_2 in living cells. Moreover, these techniques do not cause harm to the body, hence offering the possibility of real-time detection of H_2O_2 *in vivo*.

Currently, some luminescent MOFs show great potential for the detection of H_2O_2 that includes, the ZIF series,[54] the Ln-based MOFs,[8,55] the PCN series,[56,57] and the UiO series.[58,59] However, due to the lack of in-depth knowledge and design of the materials, the advantageous features of MOFs are not fully explored, which directly led to a more common detection capability. Mostakim and co-workers synthesized a new boronic acid-functionalized Zr-MOF, Zr-UiO-66-B(OH)$_2$ in 2018 by reacting ZrOCl$_2$·8H$_2$O and 2-borobenzene-1,4-dicarboxylic acid (BDC-B(OH)$_2$) in the presence of formic acid in *N,N*-dimethylacetamide (DMA) by solvothermal reaction. It is worth noting that in the presence of H_2O_2, the boronic acid functionalized ligand (BDC-B(OH)$_2$) of this material underwent selective reaction with it and the additional –B(OH)$_2$ group was converted to the –OH group. This formed Zr-UiO-66-OH, which exhibited strong fluorescence and does not undergo conversion to other ROS. This reflected the specificity of the fluorescence effect of the material on H_2O_2 and its selective detection of H_2O_2 even in the presence of other interfering ROS. This probe was highly sensitive with a detection limit of 0.015 μM, which was lower than the detection limit of other MOF-based H_2O_2 fluorescent sensors and hence can be effectively used to detect H_2O_2 in living cells.[60]

Additionally, the background auto-fluorescence effect of complex biological matrices can hinder the detection of H_2O_2 in living organisms. In 2019, Hao *et al.* synthesized a hybrid component, the assembly of which consists of an upconverted nanoparticle (UCNP) core and chiral NiS$_x$ NPs (written UCNP@ZIF-NiS$_x$)
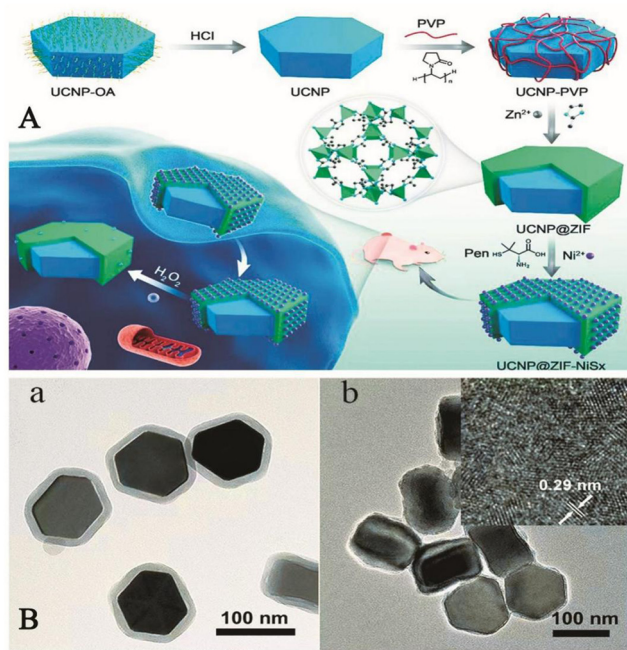
6808 | *J. Mater. Chem. B*, 2023, **11**, 6802–6822

This journal is © The Royal Society of Chemistry 2023

Fig. 6 (A) Schematic diagram of the UCNP@MOF–NiSx nanocomponent used to detect intracellular H_2O_2. (B) (a) a TEM image of the UCNP@ZIF nanostructure; (b) a TEM image of the UCNP@MOF–NiS$_x$ nanocomponent and the inset shows a high-resolution TEM image of NiS$_x$ in the nanocomponent.[61] Reproduced with permission. Copyright 2019, *Journal of the American Chemical Society*.

wrapped in a zeolite imidazole frame-8 (ZIF-8) shell. Fig. 6 shows a TEM image of the process and the structure of the component used to detect H_2O_2 *in vivo*. The experiments showed that the UCNP@ZIF-NiS$_x$ nanocomponent exhibited strong circular dichroism (CD) signals at 440 and 530 nm. However, in the presence of H_2O_2, the CD signal intensity of this component decreased and the color disappeared, which was probably due to the degradation of NiS$_x$ NPs by H_2O_2. When the concentration of H_2O_2 was between 0.05 and 20 μM, the electronic absorption spectra of this probe overlap with the green emission of UCNPs appearing at 540 nm, and the reaction of H_2O_2 with the probe led to the reduction of the absorption of the probe at 660 nm, the disappearance of the CD signal and the recovery of the luminescence signal. Even in the presence of other interfering components, there was no significant change in the CD or luminescence signal. This indicated that the probe offered good selectivity and high sensitivity. This strategy showcased the potential of chiral nanocomponents for ROS detection and provided a new idea for the development of chiral nanomaterials for biomedical and biological analysis.[61]

In summary, the fluorescence and *in vivo* luminescence properties using these materials have been shown to be highly sensitive and selective for the detection of H_2O_2 in living cells. However, there are some urgent issues that need to be addressed. First, there are sporadic reports on the fluorescent MOF-based materials that find utility as sensors for H_2O_2. Second, the fluorescence intensity of these materials is still not strong enough and needs to be further improved.

3. Application of MOFs in ion detection

Life activity is an intricate series of biological reactions involving cellular metabolism, nutrient acquisition, signal transduction and other physiological processes. It is the collective result of the involvement of many biologically active substances in various chemical reactions, of which ions are very important. These ions are involved in the formation of various enzymes or some protein carriers in the body, operation of the electron transport system, synthesis of some hormones and vitamins, the interaction with biological macromolecules such as nucleic acids, *etc.* Therefore, high as well as low concentrations of ions in the body can lead to disruption of normal physiological functions and cause various diseases. This makes the detection of ions particularly important. Different methods have been used to detect different ions, such as high performance liquid chromatography (HPLC), chemi-luminescence, anodic dissolution voltammetry (IASV), X-ray absorption spectrometry (XRD), ICP-atomic emission spectrometry (ICP-AES), ICP-mass spectrometry (ICP-MS), atomic absorption spectrophotometry (AAS), *etc.* However, their complexity, stringent requirements, high costs and high skill requirements severely limit their large-scale application. New and effective methods are therefore required that are capable of identifying and detecting heavy metal ions in samples. Also, these techniques must be simple to operate, rapid in response, sensitive and selective.[29] Hence, various nanomaterials such as gold nanoparticles, metal oxides, carbon-based nanomaterials, and polymer nanoparticles have been selectively used in this field in recent years. MOFs have received much attention due to their regular size and well-defined channel cavities.[62] Today, MOF-based materials have been developed as novel sensing materials for biomolecules and their design and synthesis has become a hot topic of research. The materials designed for the detection of different ions are not identical. In view of this, in the next section, the detection of some ions in biological systems has been covered and discussed.

3.1. MOFs for the detection of Zn^{2+}

Zn^{2+} plays a key role in many fundamental biological processes, including gene expression, neurotransmission, cell regulation and many more. Due to its unique electronic configuration, it is present in biological systems in the +2 oxidation state. Abnormal levels of Zn^{2+} may lead to chronic inflammation, dysplasia, Alzheimer's disease, *etc.* In addition, Zn^{2+} is an important indicator of the nutrient content of food.[63] Therefore, the development of a sensitive and selective probe for the detection of Zn^{2+} is of great importance. In recent years, the development in luminescence technology has opened up new avenues for the detection of this ion. By monitoring the changes in the luminescence signal, it is possible to obtain a more stable luminescence signal over time and characterized by high sensitivity, convenience and rapid response. In general, luminescent molecular systems capable of sensing Zn^{2+} cations consist of two basic parts, the Zn^{2+} binding group and the luminescent centre that can display emission. In 2018, Fan *et al.* designed a luminescent terbium metal–organic backbone TbTATB as the luminescent

sensor for Zn^{2+}. They used a tripartite planar organic ligand 4,4′,4″-triazido-2,4,6-trialkyl-tribenzoic acid (H_3TATB) as a ligand to construct luminescent MOFs with terbium that displayed unique luminescent properties of terbium due to the preferential coordination to oxygen atoms. In addition, Zn^{2+} possesses a strong coordination tendency to coordinate with nitrogen atoms and the triazine-containing ligand provides the functionalized site for Zn^{2+} detection. As expected, almost all Tb^{3+} ions were coordinated to oxygen atoms, leaving a large number of exposed Lewis basic sites. Experiments have revealed that the material has a stronger selectivity for Zn^{2+} than other competing metal ions, as well as a strong luminescence intensity and higher sensitivity. The detection limit for this sensor is 10.5 nM, which is even lower than the minimum standard level of Zn^{2+} in serum. Therefore, its ability to detect Zn^{2+} is very powerful. In addition, the material was biocompatible and capable of imaging Zn^{2+} targets in the coexistence of living cells. This sensitive and highly selective sensor therefore had the potential to be a powerful indicator of Zn^{2+} in biological systems.[64] In the same year Li *et al.* reported AuNCs/Zn-MOF nanocomposites, which can be used as fluorescent probes for the detection of Zn^{2+}. These Au nanoclusters (AuNCs) detected Zn^{2+} by aggregation-induced emission enhancement (AIEE) in aqueous media and by *in situ* formation of Zn-MOF-constrained AuNCs. This was in contrast to organic solvent-induced AuNCs aggregation and organic solvent-induced AuNCs. Instead, AuNCs were prepared by reducing tetrachloroauric acid ($HAuCl_4$) with glutathione (GSH) as a reducing and protective agent. Fluorescence experiments showed that the fluorescence quantum yield of the AuNCs/Zn-MOF composites was increased to about nine times when a certain amount of Zn^{2+} was added to the mixture of AuNCs and 2-methylimidazole (2-MIM), compared to that of single AuNCs. The material offered an extremely low detection limit of 6 nM, which provided a firm basis for its use in the determination of Zn^{2+} in human serum and hence provided an unconventional application of gold nanocluster/MOF composites in metal ion detection.[65]

Shi *et al.*, developed a nano-probe for two-photon imaging of DNAzyme-MOFs based on phosphate ion activation. As shown in Fig. 7, the strong coordination between the phosphate O and the Zr center in the MOF induced Zn^{2+}-specific RNA cleavage DNAzyme onto the MOF. This synergistic effect inhibited the extracellular activity of DNAzyme; however, upon cell entry, DNAzyme was released from the MOF by competitive binding of phosphate ions present at high intracellular concentrations. Upon release, the two-photon (TP) fluorophore-labelled DNAzyme substrate strand was cleaved in the presence of Zn^{2+}, releasing a shorter strand of DNA labelled with a TP fluorophore, thereby resulting in a strong fluorescent signal. The addition of TPF fluorophores to the nanoprobe facilitated near infrared excitation, which allowed highly sensitive and specific imaging of Zn^{2+} in live cells and tissues at greater depths than previously possible. The TP imaging capabilities facilitated the monitoring of apoptosis-related Zn^{2+} elevations in live cells and deep tissues. This phosphate ion activation strategy offers great potential for a variety of medical applications.[66]
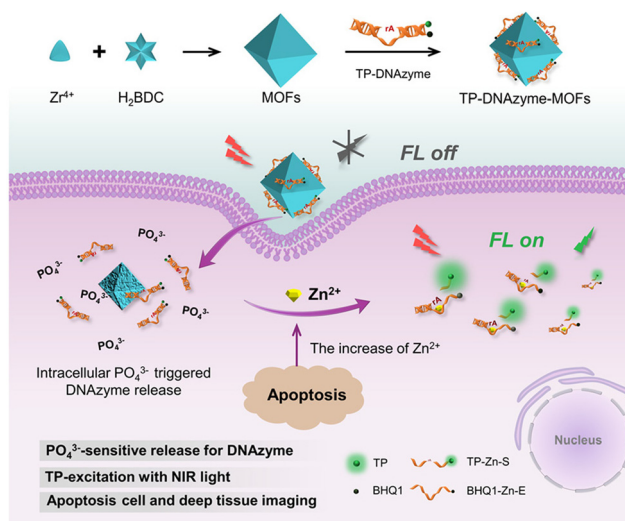

Fig. 7 The construction of the TP-DNAzyme-MOFs nanoprobe and its application in the detection of intracellular Zn^{2+} content.[66] Reproduced with permission. Copyright 2020, *ACS*.

3.2. MOFs for the detection of Fe^{2+}

Iron is one of the most abundant transition metal ions in humans and other animals. Under human physiological conditions, it is usually found in two forms, namely ferrous (Fe^{2+}) and ferric (Fe^{3+}) ions. Iron is involved in a variety of physiological processes such as oxygen transport,[67] storage metabolism,[68] electron transfer[69] and cellular respiration.[70] Both iron deficiency and its excess can have a very significant impact on the body. Iron deficiency can cause anaemia in humans, while excess iron can damage liver and kidney function, causing hepatitis and haemochromatosis. There are numerous sensors for iron, but most of them are small molecule sensors and the tendency of Fe^{2+} to oxidize under aqueous aerobic conditions impedes the detection of iron. The combination of MOFs with these sensors could improve this situation. For example, Yogesh *et al.* in 2021 developed curcumin immobilized zeolite imidazolium salt skeleton-8 (ZIF-8@Cmim) as a probe for the detection of Fe^{2+}. Curcumin has many functional groups, mainly in two mutually variable isomeric forms, namely diketones and ketoalcohols. The presence of α,β-unsaturated β-diketone groups in curcumin act as chelating agents to undergo complexation with metal ions, thus improving the water stability of curcumin in neutral and basic media. As shown in Fig. 8, when ZIF-8@Cmim, with an intrinsic fluorescent effect, binds to Fe^{2+}, Fe^{2+} binds to Cmim to form Cmim-Fe^{2+} complex and the original fluorescent effect was observed to be disrupted and the change in colour of the solution was visible to the naked eye for detection. Curcumin itself has a low solubility in aqueous media, but when loaded onto ZIF-8 its solubility increases significantly. This material has a low detection limit of 7.64 μM, which allows it to detect Fe^{2+} at the cellular level. This material was highly selective for Fe^{2+} and provided a new idea for the design of the material.[71]
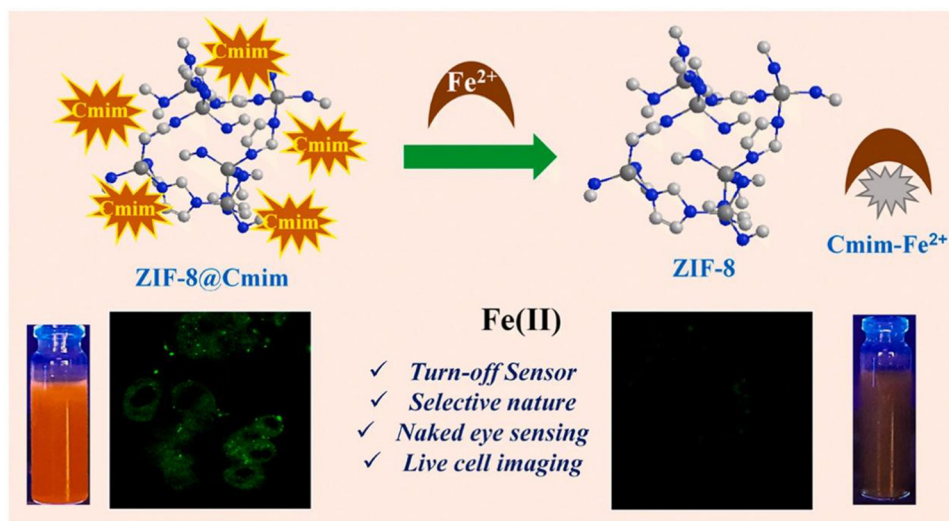
6810 | *J. Mater. Chem. B*, 2023, **11**, 6802–6822

This journal is © The Royal Society of Chemistry 2023

Fig. 8 The mechanism of action of ZIF-8@Cmim.[71] Reproduced with permission. Copyright 2021, Elsevier.

3.3. MOFs for the detection of Cu^{2+}

In our body, the concentration of Cu^{2+} ensures the appropriate functioning of organs and metabolic processes. It is an essential nutrient element in the physiological cycle. In addition, Cu^{2+} is a specific trace ion with beneficial and cytotoxic effects in various enzymatic processes and it also act as cofactors for many essential biological processes. However, the detection of Cu^{2+} is currently not an easy task, requiring either high-end instruments or complicated sample preparation methods. Recently, some new MOF-based materials have been developed and applied in practical assays.[72] Zhang *et al.* reported a dual-emission fluorescent probe Fe-MIL-88NH$_2$@RhB/Cu^{2+} based on

Fe-MIL-88NH$_2$@RhB for separate detection of Cu^{2+}/Glu and continuous detection of Glu in a highly selective and sensitive ratiometric fluorescent (RF) mode. This versatile RF probe encapsulated RhB in a Fe-MIL-88NH$_2$ porous structure, selectively recognizes Cu^{2+}/Glu based on a unique coordination principle and has good linearity with off/on fluorescence behaviour. Furthermore, Fe-MIL-88NH$_2$@RhB/Cu^{2+} when continuously treated with Glu, the quenching in fluorescence of the platform (after the perception of blue emission by Cu^{2+}) was further restored. The two characteristic emission peaks corresponding to Fe-MIL-88NH$_2$ and RhB appeared at 433 nm and 580 nm, respectively thereby confirming the successful preparation of the nanocomposite (Fig. 9A).
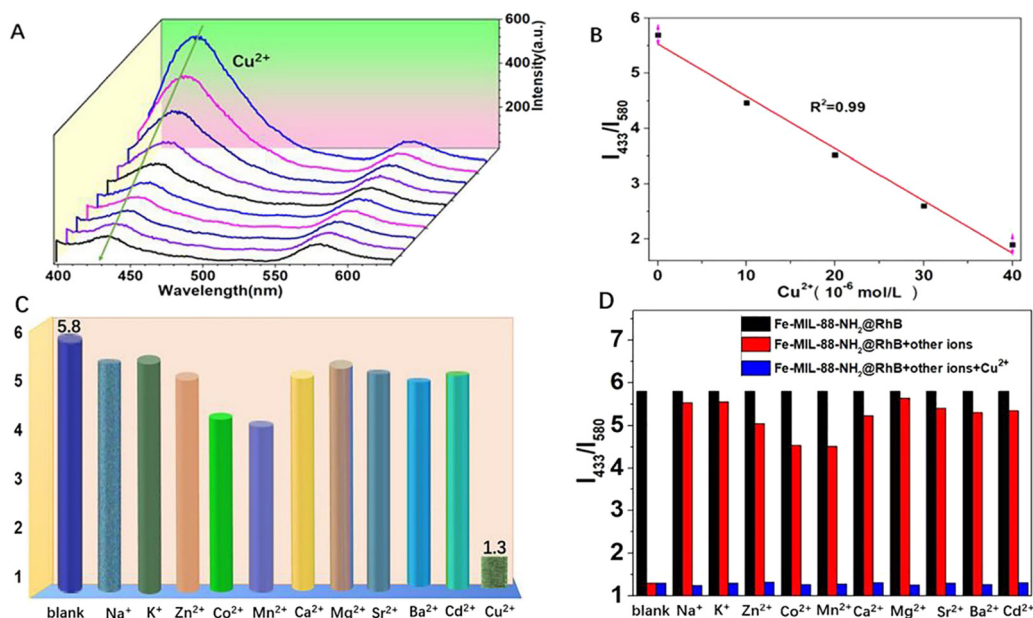

Fig. 9 (A) Luminescence spectra of Fe-MIL-88NH$_2$@RhB at different Cu^{2+} concentrations in aqueous solution. (B) Standard curve of Cu^{2+} concentration. (C) Fluorescence intensity response of Fe-MIL-88NH$_2$@RhB to other metal ions. (D) Interference test of Fe-MIL-88NH$_2$@RhB against other metal ions.[73] Reproduced with permission. Copyright 2021, Elsevier.

Whereas, the emission intensity of this probe at 433 nm dynamically decreased after the addition of Cu^{2+}, while, the fluorescence signal of the RhB molecule remained unaltered and can therefore be designated as an internal fluorescence reference. Fig. 9B shows a linear correlation between the bursting effect of Fe-MIL-88NH$_2$@RhB and the Cu^{2+} concentration. In addition, Fig. 9C estimates the selectivity of the Fe-MIL-88NH$_2$@RhB sensing system after the addition of Cu^{2+} and other analytes (Na^+, K^+, Mg^{2+}, Ca^{2+}, Zn^{2+}, Co^{2+}, Ba^{2+}, Sr^{2+}, Cd^{2+}, Mn^{2+}). It can be noted that after the addition of the other ions for more than 20 min, the change in fluorescence signal was very small and only Cu^{2+} produced a significant quenching in the fluorescence intensity. This suggested that the probe still has a good fluorescence response to Cu^{2+} even in the presence of these interfering species. Upon further addition of Cu^{2+}, its blue fluorescence at 433 nm decreased rapidly, indicating that the probe was unaffected by the other co-existing ions (Fig. 9D). The use of the Fe-MIL-88NH$_2$@RhB probe had successfully enabled the imaging of split channels of Cu^{2+} and Glu in living A549 cells with low cytotoxicity and efficient sensing of Glu in serum by molecular logic gates. This can be used for the development of medical carrier tools for the initial diagnosis of amyotrophic lateral sclerosis. Also, it has a bimodal (colour and luminescence) response for Cu^{2+} and good selectivity for this metal cation in the presence of other interfering analytes. It can be fabricated into a portable, low reading on-line test strip for the detection of Cu^{2+} with significant visual colour development.[73]

The majority of the probes discussed in the preceding sections had deep tissue penetration, good selectivity, and outstanding biosafety. All of these features make these probes extremely useful for bioassays and biological studies. But there are, however, some issues with these probes. The majority of the techniques employed for these probes are fluorescence-based, with only a few exceptions using alternative approaches. It is envisaged that additional detection technologies will arise in the future, providing even better options for the detection of these ions.

4. Application of MOFs in the detection of hydrogen sulfide

Hydrogen sulfide (H$_2$S) has been shown to be involved in a variety of physiological processes, such as immune response, angiogenesis, antioxidant, neurotransmission, and apoptosis. In recent years, studies have found that abnormal levels of hydrogen sulfide (H$_2$S) are also associated with a variety of diseases, such as diabetes, Alzheimer's disease, cirrhosis, Down's syndrome and cancer.[74] Therefore, the presence of abnormal concentrations of hydrogen sulfide (H$_2$S) in the human body is an important signal, and H$_2$S is a potential target for the identification and treatment of these diseases. The examination of H$_2$S in biological systems is of great significance for understanding its role in related physiological and pathological processes. The construction of an efficient H$_2$S detection platform has also become a new focus of research. Over the past decade, varieties of fluorescent probes

have been used for the rapid detection of H$_2$S. According to current studies, the sensing mechanism of H$_2$S detection of fluorescent probes can be divided into three categories: H$_2$S reduction reaction, H$_2$S nucleophilic reaction and metal sulfide precipitation reaction.[75–77] Due to the many excellent properties of MOF materials, in recent years, scientists have studied the application of MOF materials in the construction of efficient hydrogen sulfide (H$_2$S) detection platform. Fluorescence can be produced by using organic ligands with a tendency to absorb UV/visible light.[78] Fluorescence is the most commonly used strategy for the effective detection of H$_2$S in liquid or biological samples.[79] Nagarkar et al. firstly synthesized UiO-66@NH$_2$ using a solvothermal method, and then chemically modified the free –NH$_2$ into –N$_2$ by diazotizing –NH$_2$. Thus, the metal–organic azide framework (MOF) UiO-66@N$_3$ was obtained as a selectively opened fluorescent probe for H$_2$S detection.[80] To detect the fluorescence switching response of UiO-66@N$_3$ to H$_2$S, they excited UiO-66@N$_3$ at 334 nm and recorded the fluorescence spectra in the range of 350–650 nm. The results showed that the fluorescence reaction of the material was very weak because the electrons withdraw from the azide group and remain shut down. However, the fluorescence intensity of UiO-66@N$_3$ treated with Na$_2$S was significantly enhanced. The quantitative response of the probe UiO-66@N$_3$ towards H$_2$S was measured by fluorescence titration in HEPES buffer (10 mM and pH 7.4). The incremental addition of Na$_2$S resulted in the enhancement of the characteristic fluorescence emission peak at 436 nm. Also, the plot constructed between fluorescence intensity at 436 nm versus H$_2$S concentration showed a linear correlation. A detection limit of 118 mM for H$_2$S was obtained for UiO-66@N$_3$, which was within the range of H$_2$S concentrations in most biological systems.

In order to evaluate the response time of UiO-66@N$_3$ towards H$_2$S, the periodic fluorescence spectra were obtained (Fig. 10A). The results showed enhancement in fluorescence intensity by 16 times with $t_{1/2}$ = 13.6 s, and the reaction was completed within t_R = 180 s. This rapid response illustrated the potential of UiO-66@N$_3$ for real-time intracellular H$_2$S imaging. To demonstrate the sensing capabilities of UiO-66@N$_3$ in biological systems, they performed cytotoxicity and live cell imaging studies using HeLa cell lines. The cytotoxicity of UiO-66@N$_3$ was determined by 3-(4,5)-dimethylthiahiazo(-z-y1)-2,5-di-phenytetrazoliumromide (MTT) assay and the toxicity level of UiO-66@N$_3$ to HeLa cells was determined by different concentrations of UiO-66@N$_3$. They first incubated HeLa cells with UiO-66@N$_3$ for 6 hours after which HeLa cells still exhibited low toxicity (Fig. 10B). In cell imaging studies, very low intensity fluorescence was observed when HeLa cells were incubated with UiO-66@N$_3$ for 6 hours (Fig. 10C–E). However, strong fluorescence was observed in HeLa cells after incubation with Na$_2$S for 30 min under the same conditions (Fig. 10F–H). These results indicated that UiO-66@N$_3$ has a high selectivity and fast fluorescence initiation reaction against H$_2$S and thus, can be used to monitor H$_2$S in cells. The main mechanism behind the fluorescence turn-on response of UiO-66@N$_3$ towards H$_2$S was attributed to the reduction of a "dark" azido group to an emitting amino group. This was the first example of MOF
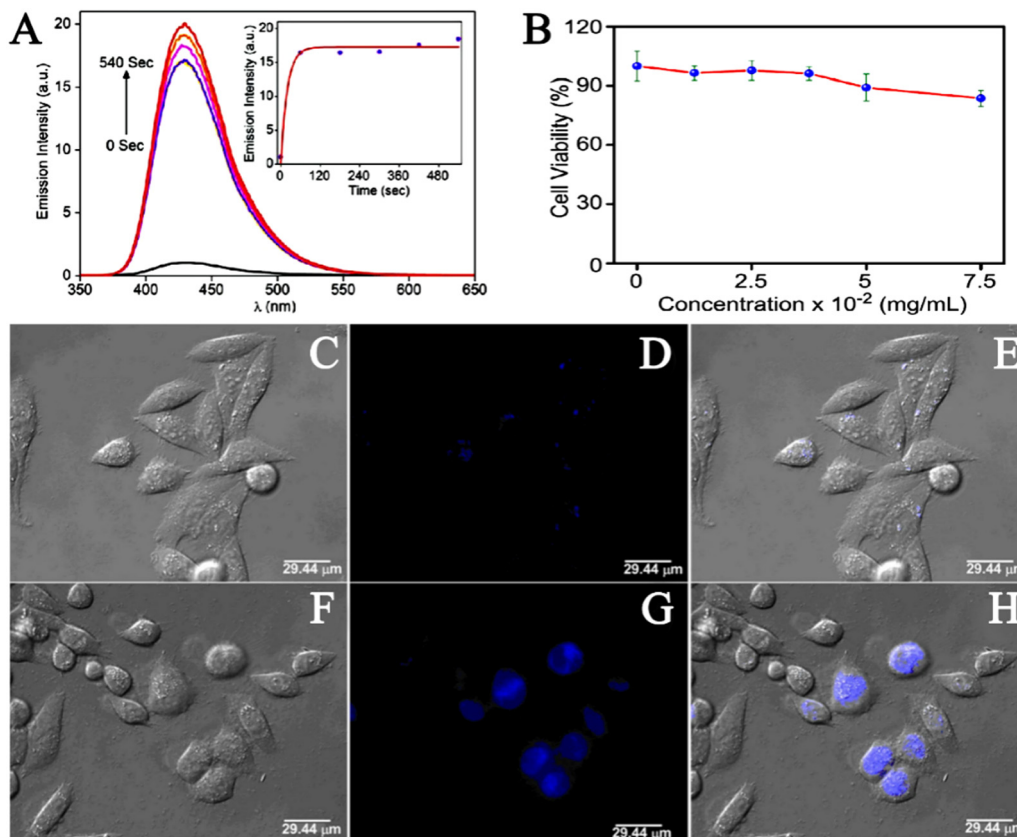
6812 | J. Mater. Chem. B, 2023, 11, 6802–6822

This journal is © The Royal Society of Chemistry 2023

Fig. 10 (A) Fluorescence response of 1-N$_3$ towards the addition of Na$_2$S after 0, 60, 180, 300, 420 and 540 seconds. Inset: Time dependence of emission intensity at 436 nm. (B) HeLa cells were treated with 1-N$_3$ before adding MTT for 6 h. Results are expressed as % of the control (100%). (C–E) Fluorescence imaging of HeLa cells incubated with 1-N3. (F–H) Fluorescence imaging of HeLa cells incubated with Na$_2$S.[80] Reproduced with permission. Copyright 2014, Springer Nature.

showing a rapid and highly selective fluorescence initiation response to H$_2$S under physiological conditions.

Xin *et al.* developed a cyclodextrin (CD)-based metal–organic nanotube (CD-MONT-2′) as a fluorescence turn-on probe for the detection of H$_2$S in living cells.[81] To investigate the fluorescence response of CD-MONT-2 to H$_2$S, they dissolved CD-MONT-2′ in DMSO to prepare 10 μM stock solutions, and then recorded the emission spectra at 350–650 nm under 330 nm excitation. The results showed that CD-MONT-2′ exhibited weak fluorescence in DMSO. When 1 mL H$_2$S was added to the stock solution, the fluorescence intensity was significantly enhanced (Fig. 11A). Furthermore, to explore the fluorescence opening response of CD-MONT-2′ to sulfide, they added different concentrations of Na$_2$S (0–10 μM) into the solution and recorded the fluorescence spectra (Fig. 11B). In order to explore the fluorescence selectivity of CD-MONT-2′, Na$_2$SO$_4$, Na$_2$S$_2$O$_3$, Na$_2$SO$_3$ and glucose, thiol amino acids and non-thiol amino acids were selected as the control group of Na$_2$S. The fluorescence intensity images of the obtained results are shown in Fig. 11C and D. These results indicated that CD-MONT-2′ has a high selectivity and moderate sensitivity fluorescence opening reaction against H$_2$S molecules. The sensing mechanism is based on the coordination between H$_2$S and the metal ion in the center of the probe to adjust the fluorescence intensity.

Fig. 11E reveals the mechanism of CD-MONT-2′ opening of fluorescent probes. During the subsequent cellular imaging experiments, they added PBS solution with different concentrations of Na$_2$S into the treated HeLa cells and analyzed the fluorescence imaging results of each group. The results showed that the CD-MONT-2′ probe not only detected the external sulfides added to the cell culture, but also sulfides produced by cells in the body. This also suggested that CD-MONT-2′ has the potential for real-time intracellular H$_2$S imaging with a highly selective and moderately sensitive fluorescence-on response to H$_2$S molecules in the cell growth environment.

Das *et al.* prepared Al-MiL-53-N$_3$ using a solvothermal method and investigated its ability to detect intracellular H$_2$S in a live cell imaging assay.[82] They first implanted a probe (25 μM) into macrophages and then treated the cells with a Na$_2$S solution (5 μM), which induced intracellular H$_2$S production. The results showed that cells loaded with probes and treated with Na$_2$S showed bright fluorescence, which suggested that the Al-MIL-53-N$_3$ probe had the ability to recognize H$_2$S in cells. Yuan *et al.* reported a novel two-mode probe based on a circular dichroic spectrum (CD) and fluorescence signal (CuxOS@ZIF-8).[83] CD is an ideal and powerful bioassay technique because it is highly sensitive and does not damage cells during the detection process. Fig. 12 shows the principle of the CuxOS@ZIF-8 nanosensor for
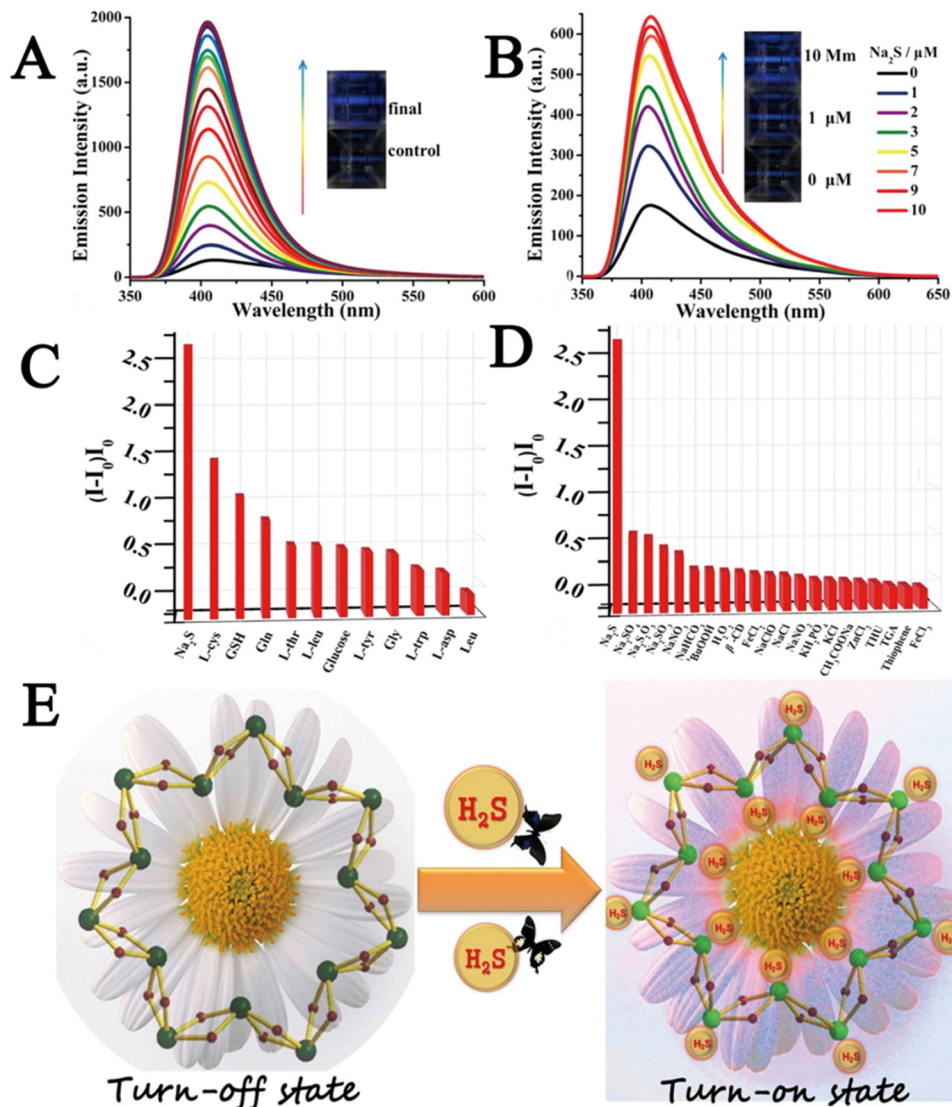
Fig. 11 (A) Schematic diagram of fluorescence intensity changing with time within 15 min of adding H_2S. (B) The fluorescence spectra of different concentrations of Na_2S (0–10 μM) were added into the culture medium. (C and D) Fluorescence intensity images of CD-MONT-2′ in different substance systems. $(I − I_0)/I_0$ (where I_0 is the initial fluorescence intensity, and I is the fluorescence intensity after the addition of the analyte). (E) Schematic diagram of the mechanism of CD-MONT-2′ opening fluorescence probe.[81] Reproduced with permission. Copyright 2016, Springer Nature.

endogenous H_2S detection. The use of ZIF-8 conferred high levels of selectivity toward H_2S. Only H_2S was allowed to react with the internal skeleton of Cu_xOS. To investigate the stability and biocompatibility of the Cu_xOS@ZIF-8 probe, they tested the probe in an environment with a pH of 5.0–7.4. In the Phosphate Buffered Saline (PBS) buffer (pH = 7.4), the hydrodynamic size of the nano-probe remained unchanged which indicated the good stability of the probe. In a biocompatibility study of CuxOS@ZIF-8, it was observed that there were few adverse effects in living cells for 48 h even at concentrations of Cu_xOS@ZIF-8 as high as 100 μg mL^{-1}, and Cu_xOS@ZIF-8 did not cause ROS reactions in HeLa cells. These results showed that the CD and fluorescence signal system created by Cu_xOS@ZIF-8 has good stability and biocompatibility, and has high selectivity and sensitivity for H_2S detection. The probe employed both CD and

fluorescence signals to accurately detect H_2S not only *in vitro*, but also in living cells and *in vivo*. In the detection process, the chiral Cu_xOS was transformed into the achiral Cu_xS, thus realizing the ultra-sensitive detection. This strategy opened up new avenues for the development of chiral nanostructures for biocatalysis, bioimaging, and diagnostics in life sciences.

To sum up, most of the current studies on the detection of H_2S by MOFs are in the stage of *in vitro* experiments, which are conducted by simulating the cell environment *in vitro*, and until now *in vivo* experiments in animals have rarely been executed. Also, most experiments are executed by adding exotic sulfides (Na_2S, H_2S). Apart from this, in order to activate the fluorescence effect of fluorescent probes, some potential sulfide sources such as GSH and L-cysteine (L-Cys) should be increased to investigate the fluorescence effect of open probes.
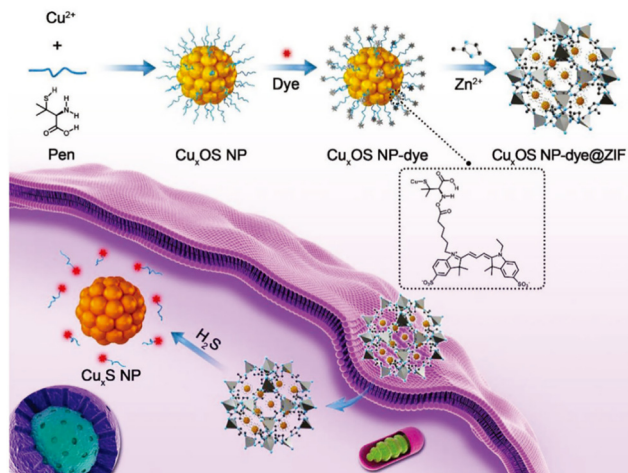
6814 | *J. Mater. Chem. B*, 2023, **11**, 6802–6822

This journal is © The Royal Society of Chemistry 2023

Fig. 12 Cu$_x$OS@ZIF-8. Schematic diagram of detecting H$_2$S in cells using a nanosensor.[83] Reproduced with permission. Copyright 2020, Wiley.

5. Application of MOFs in the detection of organic molecules

5.1. Application of MOFs in detecting GSH

Glutathione (GSH) is a tripeptide containing γ-amide bond and sulfhydryl group, composed of glutamic acid, cysteine and glycine. It is present in almost every cell of the human body. GSH is an important endogenous antioxidant,[84] which has antioxidant and detoxification effects.[85] Normal GSH levels in cells help in removing free radicals and maintain normal immune system function. The abnormal level of GSH is closely related to the occurrence and development of many serious diseases. For example, studies on the mechanisms of drug resistance have shown that the resistance is mediated by multiple factors, in which high levels of glutathione may play an important role. GSH may produce drug resistance by resisting oxidative stress, repairing DNA damage caused by chemotherapy,[86] or combining with chemotherapeutic drugs to promote the efflux of chemotherapy drugs.[87] Therefore, accurate imaging and sensing of glutathione *in vivo* is of great significance for understanding its related physiological or pathological activities, which is conducive for disease prevention or the development of new therapeutic techniques. At present, the main methods for detecting GSH in organisms are high performance liquid chromatography,[88] electrochemistry,[89] colorimetry,[90] photoelectric chemical method,[91] surface-enhanced Raman spectroscopy,[92] enzyme-linked immunosorbent,[93] and fluorescent assays.[94] Compared to other detection methods, fluorescence detection possesses non-destructive characteristics, real-time monitoring, rapid response, high selectivity and sensitivity, *etc.* Therefore, GSH detection and cell imaging have good application prospects. In recent years, scientists are attempting to use MOFs as a fluorescent platform for the detection of GSH.

Li *et al.* constructed a nanoscale metal–organic framework (Mi-UiO-66 and Mi-UiO-67) fluorescent probe for detecting Cys and GSH using a solvothermal method.[95] They uplifted the fluorescence sensing capability of the materials by introducing maleimide groups into the NMOFs, that resulted in Mi-UiO-66 and Mi-UiO-67 displaying excellent photophysical properties for biological applications. This is because incorporating organic fluorescent switches into periodic and porous NMOFs using this strategy not only effectively prevented the aggregation-induced bursts (ACQ), but also effectively prevented dye leaching. Transmission electron microscopy (TEM) showed that the size of Mi-UiO-66 and Mi-UiO-67 nanoparticles was ≤100 nm with even size distribution, which was suitable for living cell imaging. They also examined the stability of the obtained Mi-UiO-66 and Mi-UiO-67 in cell culture, and the PXRD measurements indicated that they were very stable and suitable for use in biological imaging. To explore the selectivity of Mi-UiO-66 and Mi-UiO-67 for Cys and GSH, they applied Mi-UiO-66 and Mi-UiO-67 in the presence of various interferons (Ala, Val, Leu, Ile, Pro, Phe). The fluorescent response in this environment showed that only Cys and GSH could induce significant fluorescence enhancement, indicating that Mi-UiO-66 and Mi-UiO-67 were fluorescence probes with good selectivity.

Zhu *et al.* prepared MnO$_2$ NS@Ru(bpy)$_3$$^{2+}$-UiO-66 nanocomposites coated with manganese dioxide nanosheets by an in-situ growth method as a fluorescence sensing platform for GSH in living cells.[96] They investigated the selectivity, stability and biocompatibility of MnO$_2$ NS@Ru(bpy)$_3$$^{2+}$-UiO-66 nanocomposites. First, the selectivity of this platform was evaluated by investigating the fluorescence response toward various potentially competing interferences (KCl, MgSO$_4$, FeCl$_2$, Glu, Tyr, BSA, UA, Lys, AA, Cys). The results showed that the fluorescence intensity of glutathione was significantly greater than that of other substances. These results indicated that MnO$_2$ NS@Ru(bpy)$_3$$^{2+}$-UiO-66 nanocomposites have high selectivity for GSH. In addition, the fluorescence detection of 20 μM GSH was performed for eight consecutive times with no perceptible change in the results, indicating that the fluorescence detection system has good stability. Using HeLa cells as an example, this group analyzed the biocompatibility of MnO$_2$ NS@Ru(bpy)$_3$$^{2+}$-UiO-66 by MTT assay. When HeLa cells were exposed to MnO$_2$ NS@Ru(bpy)$_3$$^{2+}$-UiO-66 at a concentration lower than 120 μg mL^{-1} for 24 h, no significant decrease in cell survival was observed. These results indicate that MnO$_2$ NS@Ru(bpy)$_3$$^{2+}$-UiO-66 has good biocompatibility and has significant application prospects in GSH detection *in vivo*.

Yang *et al.* for the first time developed a new sensitive two-photon NMOF fluorescent probe (TPNP-1) based on the host-guest interaction.[97] As shown in Fig. 13, TPNP-1 can be used to monitor fluctuations in endogenous GSH levels in living cells. They first synthesized UiO-66-NH$_2$ by solvothermal reaction. Secondly, due to the unique porous structure of UiO-66-NH$_2$, which possess excellent surface negative potential and has excellent adsorption ability on cationic dyes, they opted to introduce DMASM dye to UiO-66-NH$_2$, which provided the two-photon fluorescence system DMASM ⊂ UiO-66-NH$_2$. Finally the KMnO$_4$ solution of different concentrations (50, 100, 150, 200, 250 μg mL^{-1}) was introduced into the DMASM ⊂ UiO-66-NH$_2$ in aqueous medium with strong stirring at room temperature that yielded TPNP-1.

In the cell experiment, considering the difference in GSH content between cancer cells and normal cells, HepG2, HeLa
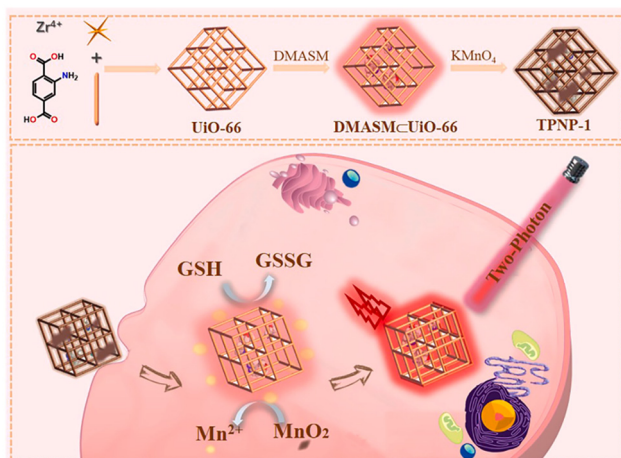
This journal is © The Royal Society of Chemistry 2023

J. Mater. Chem. B, 2023, **11**, 6802–6822 | **6815**

Fig. 13 Schematic diagram of TPNP-1 detecting intracellular GSH.[97] Reproduced with permission. Copyright 2021, Elsevier.

and normal hepatocyte L02 cells were selected for the GSH *in situ* fluorescence imaging experiment (Fig. 14A–I).

After incubating different cell lines and probe TPNP-1 for 4 hours in DMEM medium of 37 °C, they excited the two photon confocal images at 880 nm using a nanosecond laser (Fig. 15A and B). Thereafter, TPNP-1 was applied to tissue imaging of mouse liver sections. The liver sections were first incubated

with PBS solution containing TPNP-1 for 30 min, and then the fluorescence intensity changes at different scanning depths were recorded using a two-photon microscope under Z-scan mode. Imaging showed (Fig. 15C) that two-photon fluorescence imaging of rat liver sections showed a penetration depth of 170 nm with a detection limit of 87 nM. The results showed that the two-photon imaging based on the probe can be realized not only in living cells, but also in deep living tissues. The construction of the TPNP-1 two-photon fluorescence probe effectively solved the problem of poor penetration of a single photon fluorescence probe into biological tissue.

5.2. Application of MOFs in nucleic acid detection

MicroRNA (miRNA) is a class of endogenous small RNAs with 20–24 nucleotides in length. It plays a variety of important regulatory roles in cells and is involved in a series of important processes during life, including early development, cell proliferation, apoptosis, cell death, lipid metabolism and cell differentiation. In addition, miRNAs are considered to be biomarkers closely related to cell carcinogenesis,[98] and an emerging diagnostic and prognostic biomarker. Therefore, it is of great significance to develop a reliable sensing strategy to monitor miRNA in living cells. Conventional miRNA detection methods include northern blotting,[99] real-time quantitative PCR,[100] and microarrays.[101] However, none of these methods
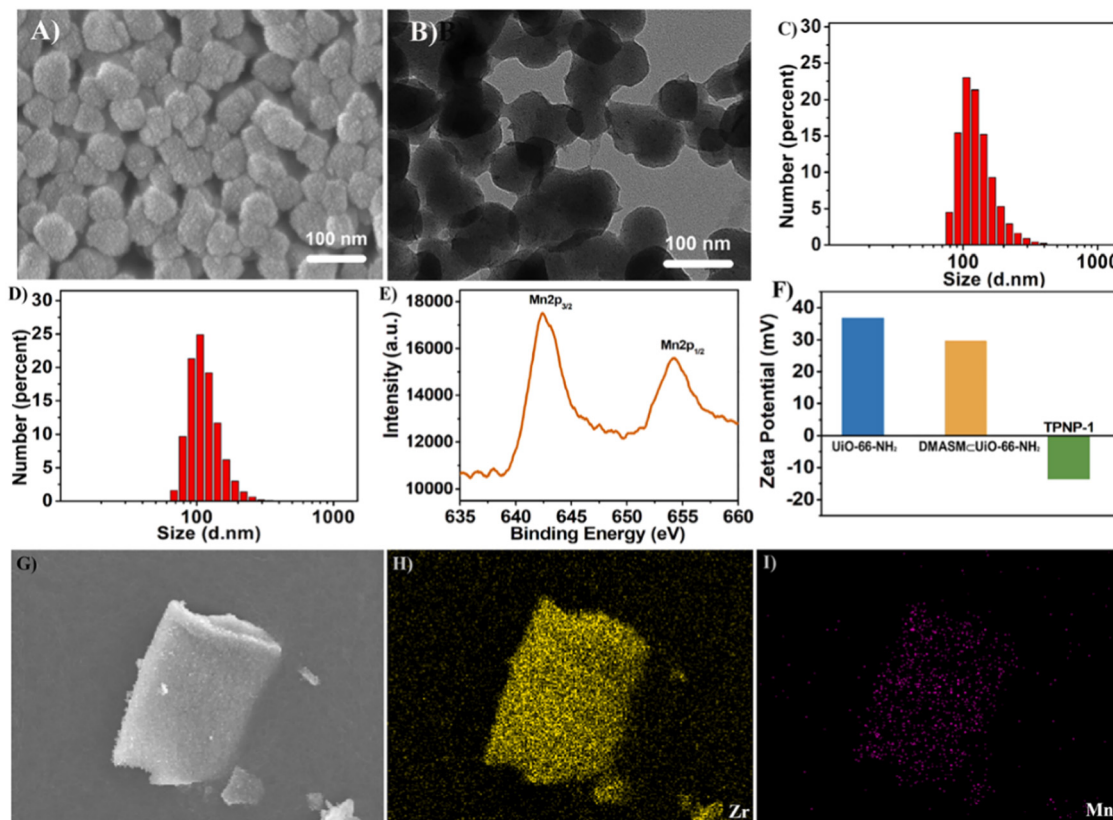

Fig. 14 (A) SEM image of TPNP-1 (scale bar = 100 nm). (B) TEM image of TPNP-1 (scale bar = 100 nm). (C) DLS data of TPNP-1. (D) DLS data of DMASM⊂UiO-66-NH$_2$. (E) XPS plot of TPNP-1. (F) Zeta potential diagram for UiO-66-NH$_2$, DMASM⊂UiO-66-NH$_2$ and TPNP-1. (G–I) SEM-mapping image of TPNP-1.[97] Reproduced with permission. Copyright 2021, Elsevier.

6816 | *J. Mater. Chem. B*, 2023, **11**, 6802–6822

This journal is © The Royal Society of Chemistry 2023

could monitor the miRNA level expressed in living cells in real time, and they also have different shortcomings. Therefore, it is of great significance to develop some new methods that are more sensitive and selective for the detection of miRNA in cells. In recent years, many scientific groups have employed MOFs for the construction of an miRNA detection platform to improve the stability, biocompatibility, sensitivity and other advantages of the detection platform.

Traditional miRNA assays are unable to monitor miRNA levels in living cells in real time. Wu *et al.* constructed a novel fluorescent biosensor (PANMOF) based on a fluorophore-labeled peptide nucleic acid (PNA) probe combined with an NMOF (UiO-66) vector for monitoring multiplexed miRNAs in live cancer cells (Fig. 16).[102] This miRNA sensor not only enabled quantitative and highly specific detection of multiple miRNAs in living cancer cells, but also allowed precise and *in situ* monitoring of spatial and temporal changes in miRNA expression. When the PNA probe was firmly bound to the nanoporous NMOF carrier, the fluorescence of dye-labelled PNAs was dramatically burst.[103] However, in the presence of targeted miRNAs, the dye-labelled PNAs were released from the NMOF and hybridized with the target miRNAs, resulting in a recovery of fluorescence of the PNA probe. They first validated the effectiveness of the proposed miRNA sensing scheme using the PANMOF platform in homogeneous solution. Preliminary experiments showed that PANMOF can be used as a bio-sensing platform for miRNAs. Thereafter, they applied the PANMOF system to two human breast cancer cells, MCF-7 and MDA-MB-231, for miRNA detection studies. The cultured cells were first incubated with the FAM-PNA21-NMOF complex (a PANMOF complex) for 14 hours.

Earlier studies have shown that NMOF nanoparticles can be internalized into biological cells through phagocytosis that resulted in bright fluorescence of the FAM-PNA21-NMOF complex (Fig. 17) showing the fluorescence intensity exhibited
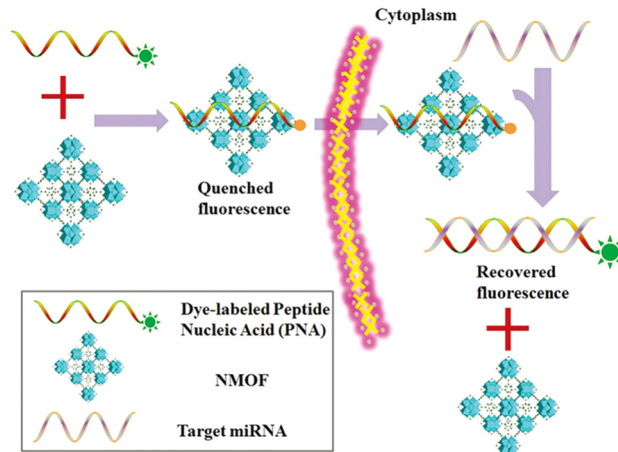

Fig. 16 Schematic diagram of the PANMOF sensing mechanism.[102] Reproduced with permission. Copyright 2015, RSC.

by different cell lines after incubation. In addition, they explored the potential cytotoxicity of PANMOF by MTT assay. The results showed that two cancer cells retained more than 90% of their activity after treatment with PANMOF at concentrations of up to $80~\mu g~mL^{-1}$, which indicated its excellent biocompatibility. In summary, the PANMOF bio-sensing platform possesses excellent sensitivity, specificity and biocompatibility, providing an important method for monitoring the dynamic changes of miRNA expression in living cancer cells.

Hu *et al.* reported a bimetallic organic backbone (CoNi-MOF) using a solvothermal method,[104] as an efficient sensing platform for miRNA-126 detection. Compared to the homo-structured monometallic Co-MOF or Ni-MOF, the bimetallic CoNi-MOF exhibited superior electrochemical activity due to the synergistic interaction between multiple metal centres and electrochemically active ligands. They tested CoNi-MOF for selectivity as well as
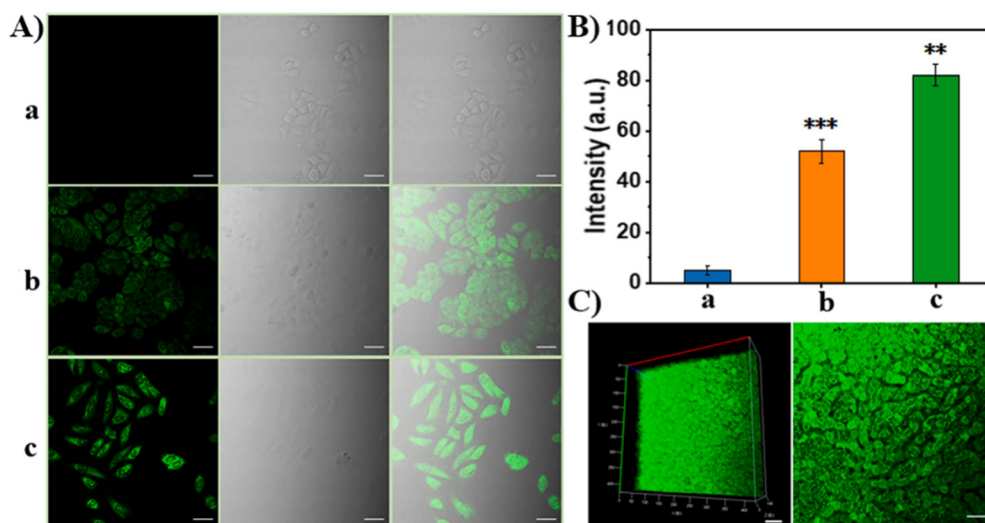

Fig. 15 (A) Fluorescence images of HeLa cells: (a) $50~\mu g~mL^{-1}$ TPNP-1 after $500~\mu M$ NEM incubated; (b) $50~\mu g~mL^{-1}$ TPNP-1; (c) $50~\mu g~mL^{-1}$ TPNP-1 after $200~\mu M$ LPA incubated; (B) relative fluorescence intensities of *a*, *b* and *c*; (C) two photon fluorescence images of fresh mice liver tissue slice.[97] Reproduced with permission. Copyright 2021, Elsevier.

This journal is © The Royal Society of Chemistry 2023

J. Mater. Chem. B, 2023, **11**, 6802–6822 | **6817**

stability and in the presence of multiple interferers (MM1, MM2, miRNA-141, miRNA-155 and miRNA-21) and it displayed high selectivity for miRNA-126, which could be attributed to the efficient and specific hybridization. Also, the measurement using the miRNA-126/cDNA/CoNi-MOF(1:1)/AE based electrode was executed continuously for 15 days and the results showed that the electrochemical impedance spectroscopy (ESI) response did not change significantly throughout the experiment, thereby demonstrating the good stability of miRNA-126/cDNA/CoNi-MOF. Notably, they also tested the miRNA-126/cDNA/CoNi-MOF for reusability, where they probed the reusability of the biosensor CoNi-MOF by measuring miRNA-126 (10 pm) detection at five separate electrodes. The data showed a low RSD of 1.01% for the EIS response, and after refreshing again, the EIS returned to the original level, which demonstrated the reusable nature of the biosensor CoNi-MOF.

Yang *et al.* reported a novel two-photon nanoprobe TP-CHA-UiO-66,[105] using MOF as a nanocarrier and hairpins as a two-photon fluorescent signal amplifier for miRNA imaging of tumour cells and deep tissues. Where TP was a fluorophore, and its excellent imaging performance could facilitate and boost imaging of tumour-associated miRNAs in live tumour cells and tissues. Catalytic hairpin assembly (CHA),[106] was an ultra-sensitive and highly efficient selective RNA amplification detection strategy that identified the target and amplifies the signal. Fig. 18A illustrates the imaging process of TP-CHA-UiO-66 in live cancer cells. Upon penetration into the cell, intracellular phosphate coordinated with the Zr atoms of the MOF, thereby leading to the release of hairpins on the surface of TP-CHA-MOFs. The intracellular miRNA triggered

the formation of H1-H2 duplex structures, leading to the switching mode of the TP fluorescent signal and enabling the amplification and detection of the target miRNA. After the preparation and characterization of TP-CHA-MOFs, investigators performed *in vitro* fluorescence imaging experiments as well as intracellular fluorescence imaging experiments on TP-CHA-MOFs. In an *in vitro* fluorometric assay, they dispersed TP-CHA-MOF nanoprobes (10 μL, 1 μM DNA) in a phosphate-buffered solution (PBS, 10 mM, pH = 7.4) similar to the cellular environment for 6 h at 37 °C, then added miRNA-21 (0–120 nM) at different concentration gradients to this mixture and incubated for 1.5 h at 37 °C. Fluorescence spectra were recorded at 400 nm excitation wavelength and the same experiments were then performed under the same conditions in HEPES and Tris buffers. As shown in Fig. 18B, only weak fluorescent emission was observed in HEPES and Tris buffers containing miRNA-21, whereas intense fluorescent emission resulted in PBS buffer due to phosphate triggering the release of H1 and H2 from MOFs. These results demonstrated the good selectivity of the TP-CHA-MOFs fluorescent probe for the PBS buffer solution, which indirectly indicated that the TP-CHA-MOFs fluorescent probe can be applied within the cellular
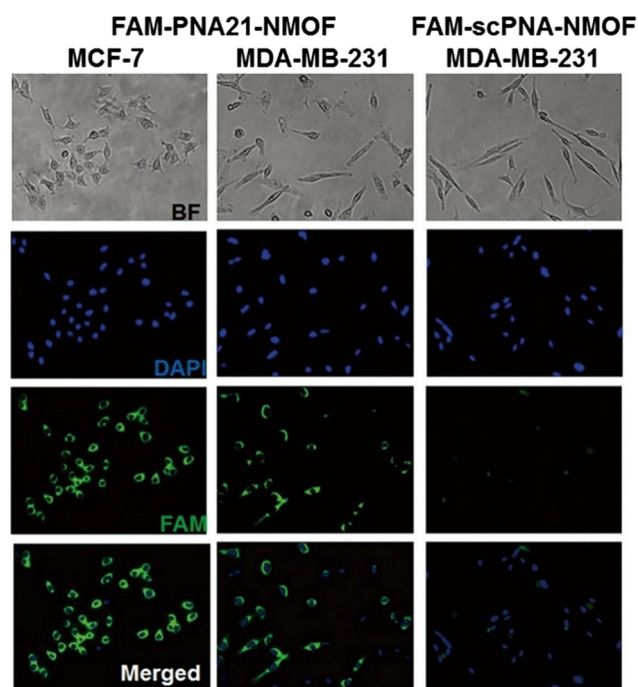

Fig. 17 Fluorescence images obtained after 14 h incubation with FAM-PNA21-NMOF and FAM-scPNA-NMOF.[102] Reproduced with permission. Copyright 2015, RSC.
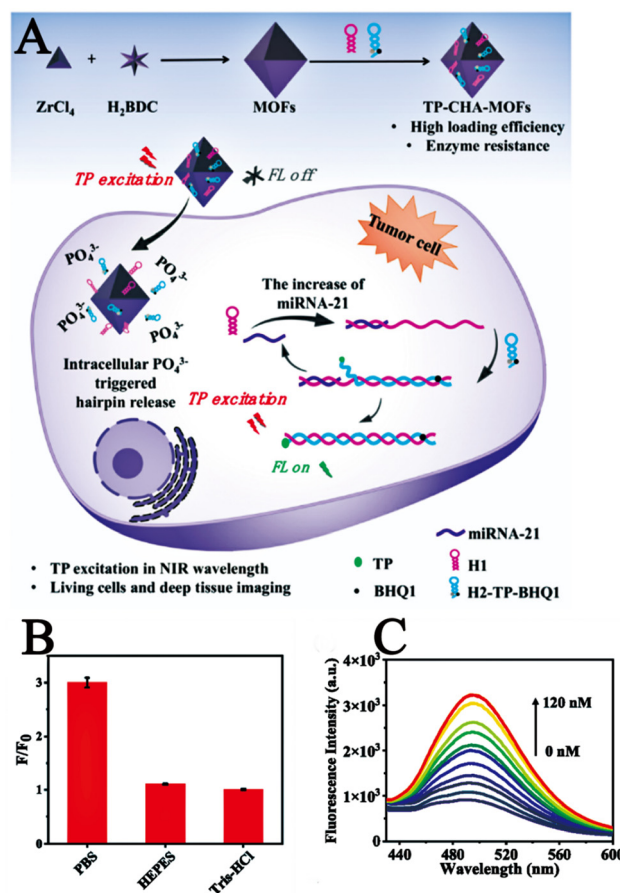

Fig. 18 (A) Schematic diagram of the imaging process of TP-CHA-UiO-66 in living cells. (B) F/F_0 for TP-CHA-MOFs incubated with miRNA in DPBS, HEPES, or Tris−HCl buffer. (C) Fluorescence spectra of various concentrations of miRNA (0−120 nM).[105] Reproduced with permission. Copyright 2022, Elsevier.

6818 | *J. Mater. Chem. B*, 2023, **11**, 6802–6822

This journal is © The Royal Society of Chemistry 2023

environment due to the presence of phosphate in the PBS buffer similar to the intracellular environment. Subsequently, they examined the *in vitro* fluorescence sensing performance of TP-CHA-MOFs nano-probes by recording the fluorescence spectra at different concentrations of TP-CHA-MOFs nanoprobes (Fig. 18C). The fluorescence intensity gradually increased as the miRNA-21 concentration increased from 0 to 120 nM. In intracellular imaging experiments, they used the CCK-8 method to investigate the cytotoxicity of TP-CHA-MOFs nanoprobes on living cells. HEK293, HeLa and MCF-7 cells were incubated with different concentrations of TP-CHA-MOFs. At the end of the incubation, the cellular activity was still over 88% which demonstrates the good biocompatibility of the TP-CHA-MOFs nanoprobes. Compared to conventional single-photon fluorescent probes, the two-photon fluorescent probe TP-CHA-UiO-66 offered better penetration and enabled fluorescence imaging in deeper biological tissues. The TP-CHA-UiO-66 nanoprobe enabled efficient TP fluorescence imaging of deep miRNA-21 in tumour tissues at penetration depths of 20–160 μm.

Compared with previously reported fluorescent probes for miRNA detection, the two-photon nanoprobe TP-CHA-UiO-66 reported by Yang *et al.* exhibited better selectivity, biocompatibility and penetration, which significantly improved the efficiency of miRNA detection and has promising applications in medical diagnostics.

In summary, investigation on the construction of miRNA biosensing platforms for detection is still at a preliminary stage. Most of the studies have been conducted only with *in vitro* fluorescence experiments and cellular experiments, while *in vivo* experiments on animals are relatively rare. The limits of detection of miRNAs with the fluorescent probes constructed so far are relatively low, and the stability of the probes needs to be improved.

6. Conclusions

This perspective reviewed the recent developments in the use of MOF materials as probes and biosensing platforms for diverse chemicals (H_2O_2, metal ions, H_2S, GSH, and nucleic acids) in biological cells. These MOF-based biological probes offer better sensitivity, good biocompatibility, and targeting features than traditional detection probes, which considerably improves the precision of detection. However, many problems need to be addressed appropriately. For example, the design and development of new MOF-based materials as probes for such biochemical analytes are still required. This is because, the majority of MOFs utilized to build bio-probes in recent years have been based on UiO-66. Furthermore, the sensitivity and selectivity of certain MOF-based bio-probes for the detection of H_2O_2 are still insufficient for the detection of extracellular hydrogen peroxide concentrations, and the detection limit range is insufficient. The shortcomings/limitations associated with the presently reported MOF-based biofluorescent probes need attention for their widespread application in the future. Perhaps a hybrid of microfluidic chips and electrochemical sensors might be examined, allowing for cell adhesion and growth. The benefits of

MOFs may be leveraged by using more than one type of MOF, and the sensor can be provided by employing a multi-MOF method to detect the analytes with appropriate sensitivity outside the cell. Conclusively, the rational design, development and fabrication of biosensors based on MOFs for the effective detection of cellular components is crucial in the biomedical field, despite the fact that there are numerous obstacles and a long way to go.

Conflicts of interest

There are no conflicts to declare.

Acknowledgements

References

1 H. Cui, S. Cui, S. Zhang, Q. Tian, Y. Liu, P. Zhang, M. Wang, J. Zhang and X. Li, *Analyst*, 2021, **146**, 5951–5961.

2 P. Zhao, S. Chen, J. Zhou, S. Zhang, D. Huo and C. Huo, *Anal. Chim. Acta*, 2020, **1128**, 90–98.

3 Y. Li, P. Zhang, Z. Ouyang, M. Zhang, Z. Lin, J. Li, Z. Su and G. Wei, *Adv. Funct. Mater.*, 2016, **26**, 2122–2134.

4 L. García-Carmona, M. Moreno-Guzmán, A. Martín, S. B. Martínez, A. B. Fernández-Martínez, M. C. González, J. Lucio-Cazaña and A. Escarpa, *Biosens. Bioelectron.*, 2017, **96**, 146–151.

5 J. Huang, H. Li, Y. Zhu, Q. Cheng, X. Yang and C. Li, *J. Mater. Chem. A*, 2015, **3**, 8734–8741.

6 J. Bai and X. E. Jiang, *Anal. Chem.*, 2013, **85**, 8095–8101.

7 Y. Zhang, J. Xiao, Y. Sun, L. Wang, X. Dong, J. Ren, W. He and F. Xiao, *Biosens. Bioelectron.*, 2018, **100**, 453–461.

8 (*a*) H. Furukawa, K. E. Cordova, M. O'Keeffe and O. M. Yaghi, *Nature*, 2013, **341**, 1230444; (*b*) Y. N. Zeng, G. H. Xu, X. Y. Kong, G. M. Ye, J. Guo, C. Y. Lu, A. Nezamzadeh-Ejhieh, M. S. Khan, J. Q. Liu and Y. Q. Peng, *Int. J. Pharm.*,

2022, **627**, 122228; (*c*) S. Liu, Y. Z. Qiu, Y. F. Liu, W. F. Zhang, Z. Dai, D. Srivastava, A. Kumar, Y. Pan and J. Q. Liu, *New J. Chem.*, 2022, **46**, 13818–13837; (*d*) C. Y. Rao, D. H. Liao, Y. Pan, Y. Y. Zhong, W. F. Zhang, Q. Ouyang, A. Nezamzadeh-Ejhieh and J. Q. Liu, *Expert Opin. Drug Delivery*, 2022, **19**(10), 1183–1202; (*e*) X. L. Tan, D. H. Liao, C. Y. Rao, L. Y. Zhou, Z. C. Tan, Y. Pan, A. Singh, A. Kumar, J. Q. Liu and B. H. Li, *J. Solid State Chem.*, 2022, **314**, 123352; (*f*) Q. J. Ding, Z. J. Xu, L. Y. Zhou, C. Y. Rao, W. M. Li, M. Muddassir, H. Sakiyama, B. L. Q. Ouyang and J. Q. Liu, *J. Colloid Interface Sci.*, 2022, **621**, 180–194.

9 (*a*) J. Li, Ryan J. Kuppler and H. Zhou, *Chem. Soc. Rev.*, 2009, **38**, 1477–1504; (*b*) M. Y. Zeng, J. Y. Chen, L. Zhang, Y. Cheng, C. Y. Lu, Y. F. Liu, A. Singh, M. Trivedi, A. Kumar and J. Q. Liu, *Mater. Today. Commun.*, 2022, **31**, 103514; (*c*) M. M. Li, S. H. Yin, M. Z. Lin, X. L. Chen, Y. Pan, Y. Q. Peng, J. B. Sun, A. Kumar and J. Q. Liu, *J. Mater. Chem. B*, 2022, **10**, 5105–5128; (*d*) R. Q. Zheng, J. R. Guo, X. Y. Cai, L. J. Bin, C. Y. Lu, A. Singh, M. Trivedi, A. Kumar and J. Q. Liu, *Colloids Surf., B*, 2022, **213**, 112432.

10 J. Lee, J. Kim and T. Hyeon, *Adv. Mater.*, 2006, **18**, 2073–2094.

11 (*a*) D. Wang and E. Sun, *Microporous Mesoporous Mater.*, 2020, **299**, 110131; (*b*) Y. F. Wang, C. J. Wang, Q. Z. Feng, J. J. Zhai, S. S. Qi, A. G. Zhong, M. M. Chu and D. Q. Xu, *Chem. Commun.*, 2022, **58**, 6653–6656; (*c*) H. Y. Sun, S. X. Chen, A. G. Zhong, R. Sun, J. J. Jin, J. H. Yang, D. Z. Liu, J. F. Niu and S. L. Lu, *Molecules*, 2023, **28**, 3282.

12 (*a*) J. D. Obayemi, S. M. Jusu, A. A. Salifu, S. Ghahremani, M. Tadesse, V. O. Uzonwanne and W. O. Soboyejo, *Mater. Sci. Eng. C*, 2020, **112**, 110794; (*b*) Q. Z. Yang, Y. J. Wen, A. G. Zhong, J. Xu and S. J. Shao, *New J. Chem.*, 2020, **44**, 16265–16268; (*c*) S. Y. Liu, W. Q. Liu, C. X. Yuan, A. G. Zhong, D. M. Han, B. Wang, M. N. Shah, M. M. Shi and H. Z. Chen, *Dyes Pigm.*, 2016, **134**, 139–147.

13 L. E. Kreno, K. Leong, O. K. Farha, M. Allendorf, R. P. Van Duyne and J. T. Hupp, *Chem. Rev.*, 2012, **112**, 1105–1125.

14 Z. Rahmati, R. Khajavian and M. Mirzaei, *Inorg. Chem. Front.*, 2021, **8**, 3581–3586.

15 A. Zuliani, N. Khiar and C. Carrillo-Carrión, *Anal. Bioanal. Chem.*, 2023, **415**, 2005–2023.

16 (*a*) M. Bazargan, F. Ghaemi, A. Amiri and M. Mirzaei, *Coord. Chem. Rev.*, 2021, **445**, 214107; (*b*) P. Yan, X. Li, D. Y. Ma, L. J. Li, Y. W. Lan, Z. Y. Li, X. T. Lu, M. Q. Yang and F. L. Liang, *J. Solid State Chem.*, 2022, **316**, 123566; (*c*) L. Qin, Y. Li, D. Y. Ma, F. L. Liang, L. D. Chen, C. Y. Xie, J. Y. Lin, Y. N. Pan, G. Z. Li, F. R. Chen, P. R. Xu, C. L. Hong and J. X. Zhu, *J. Solid State Chem.*, 2022, **312**, 123175.

17 M. Bazargan, M. Mirzaei, A. Amiri and C. Ritchie, *Microchim. Acta*, 2021, **108**, 188.

18 J. Wang, C. Wang and W. Lin, *ACS Catal.*, 2012, **2**, 2630–2640.

19 (*a*) Y. Y. Li, D. Q. C. Li, T. R. Qin, Z. Shi, P. K. Fu, D. Q. Xiong and X. Y. Dong, *Appl. Organomet. Chem.*, 2023, **37**, e6920; (*b*) X. Y. Dong, Z. Shi, D. Q. C. Li, Y. Y. Li, N. An, Y. J. Shang, H. Sakiyama, M. Muddassir

and C. D. Si, *J. Solid State Chem.*, 2023, **318**, 123713; (*c*) T. R. Qin, Z. Shi, W. J. Zhang, X. Y. Dong, N. An, H. Sakiyama, M. Muddassir, D. Srivastava and A. Kumar, *J. Mol. Struct.*, 2023, **1282**, 135220.

20 (*a*) P. R. Lakshmi, P. Nanjan, S. Kannan and S. Shanmugaraju, *Coord. Chem. Rev.*, 2021, **435**, 213793; (*b*) Y. Shu, Q. Ye, T. Dai, Q. Xu and X. Hu, *ACS Sens.*, 2021, **6**, 641–658; (*c*) L. E. Kreno, K. Leong, O. K. Farha, M. Allendorf, R. P. Van Duyne and J. T. Hupp, *Chem. Rev.*, 2012, **112**, 1105–1125.

21 Y. Feng, Y. Wang and Y. Ying, *Coord. Chem. Rev.*, 2021, **446**, 214102.

22 (*a*) Y. Y. Zhong, Z. X. Peng, Y. Q. Peng, B. Li, Y. Pan, Q. Ouyang, H. Sakiyama, M. Muddassir and J. Q. Liu, *J. Mater. Chem. B*, 2023, DOI: **10.1039/D3TB00749A**; (*b*) W. P. Chen, M. Liu and H. P. Yang, *Pharmaceutics*, 2023, **15**, 1323; (*c*) X. L. Chen, M. M. Li, M. Z. Lin, C. Y. Lu, A. Kumar, Y. Pan, J. Q. Liu and Y. Q. Peng, *J. Mater. Chem. B*, 2023, DOI: **10.1039/D3TB00267E**; (*d*) J. Y. Chen, Z. X. Zhang, J. X. Ma, A. Nezamzadeh-Ejhieh, C. Y. Lu, Y. Pana, J. Q. Liu and Z. Bai, *Dalton Trans.*, 2023, **52**, 6226–6238; (*e*) Z. J. Xu, Z. Y. Wu, S. Huang, K. H. Ye, Y. H. Jiang, J. Q. Liu, J. C. Liu, X. W. Lu and B. Li, *J. Controlled Release*, 2023, **354**, 615–625.

23 M. Nazari, A. S. Saljooghi, M. Ramezani, M. Alibolandi and M. Mirzaei, *J. Mater. Chem. B*, 2022, **10**, 8824–8851.

24 X. Fu, B. Ding and D. D'Alessandro, *Coord. Chem. Rev.*, 2023, **475**, 214814.

25 D. I. Osman, S. M. El-Sheikh, S. M. Sheta, O. I. Ali, A. M. Salem, W. G. Shousha, S. F. El-Khamisy and S. M. Shawky, *Biosens. Bioelectron.*, 2019, **141**, 111451.

26 T. Liu, R. Hu, Y. Liu, K. Zhang, R. Bai and Y. Yang, *Microchim. Acta*, 2020, **187**, 320.

27 N. Wei, M. Y. Zhang, X. N. Zhang, G. M. Li, X. D. Zhang and Z. B. Han, *Cryst. Growth Des.*, 2014, **14**, 3002–3009.

28 (*a*) S. H. Jung, H. Lee, M. L. Seo and J. H. Jung, *Bull. Korean Chem. Soc.*, 2013, **34**, 1583–1585; (*b*) F. Ke, A. Pan, J. Q. Liu, X. X. Liu, T. Yuan, C. Y. Zhang, G. N. Fu, C. Y. Peng, J. F. Zhu and X. C. Wan, *J. Colloid Interface Sci.*, 2023, **642**, 61–68.

29 H. Sohrabi, S. Ghasemzadeh, S. Shakib, M. R. Majidi, A. Razmjou, Y. Yoon and A. Khataee, *Ind. Eng. Chem. Res.*, 2023, **62**, 4611–4627.

30 H. Zheng, C. Liu, X. Zeng, J. Chen, J. Lü, R. Lin, R. Cao, Z. Lin and J. Su, *Inorg. Chem.*, 2018, **57**, 9096–9104.

31 C. Guo, M. Hu, Z. Li, F. Duan, L. He, Z. Zhang, F. Marchetti and M. Du, *Sens. Actuators, B*, 2020, **309**, 127821.

32 F. Yu, X. Han and L. Chen, *Chem. Commun.*, 2014, **50**, 12234–12249.

33 Ü. Anik, S. Timur and Z. Dursun, *Microchim. Acta*, 2019, **186**, 196.

34 M. Hu, S. A. A. Razavi, M. Piroozzadeh and A. Morsali, *Inorg. Chem. Front.*, 2020, **7**, 1598–1632.

35 R. S. Balaban, S. Nemoto and T. Finkel, *Cell*, 2005, **120**, 483–495.

36 K. B. Beckman and B. N. Ames, *Physiol. Rev.*, 1998, **78**, 547–581.

37 T. Finkel, M. Serrano and M. A. Blasco, *Nature*, 2007, **448**, 767–774.

6820 | *J. Mater. Chem. B*, 2023, **11**, 6802–6822

This journal is © The Royal Society of Chemistry 2023

38 J. P. Fruehauf and F. L. Meyskens, *Clin. Cancer Res.*, 2007, **13**, 789–794.

39 N. Houstis, E. D. Rosen and E. S. Lander, *Nature*, 2006, **440**, 944–948.

40 D. Jay, H. Hitomi and K. K. Griendling, *Free Radical Biol. Med.*, 2006, **40**, 183–192.

41 M. P. Mattson, *Nature*, 2004, **430**, 631–639.

42 M. T. Lin and M. F. Beal, *Nature*, 2006, **443**, 787–795.

43 B. Balasubramanian, W. K. Pogozeldki and T. D. Tullius, *Proc. Natl. Acad. Sci. U. S. A.*, 1998, **95**, 9738–9743.

44 C. Li, R. Wu, J. Zou, T. Zhang, S. Zhang, Z. Zhang, X. Hu, Y. Yan and X. Ling, *Biosens. Bioelectron.*, 2018, **116**, 81–88.

45 Y. Sun, M. Luo, X. Meng, J. Xiang, L. Wang, Q. Ren and S. Guo, *Anal. Chem.*, 2017, **89**, 3761–3767.

46 W. Huang, Y. Xu, Z. Wang, K. Liao, Y. Zhang and Y. Sun, *Talanta*, 2022, **249**, 123612.

47 J. Liu, X. Bo, J. Yang, D. Yin and L. Guo, *Sens. Actuators, B*, 2017, **248**, 207–213.

48 J. Lu, Y. Hu, P. Wang, P. Liu, Z. Chen and D. Sun, *Sens. Actuators, B*, 2020, **311**, 127909.

49 H. Wang, W. Chen, Q. Chen, N. Liu, H. Cheng and T. Li, *Electroanal. Chem.*, 2021, **897**, 115603.

50 Q. Wang, Y. Yang, F. Gao, J. Ni, Y. Zhang and Z. Lin, *ACS Appl. Mater. Interfaces*, 2016, **8**, 32477–32487.

51 L. Chen, T. Wang, Y. Xue, X. Zhou, J. Zhou, X. Cheng, Z. Xie, Q. Kuang and L. Zheng, *Adv. Mater. Interfaces*, 2018, **5**, 1801168.

52 S. Zhou, L. Jiang, J. Zhang, P. Zhao, M. Yang, D. Huo, X. Luo, C. Shen and C. Hou, *Mikrochim. Acta, Suppl.*, 2021, **188**, 160.

53 X. Yang, W. Qiu, R. Gao, Y. Wang, Y. Bai, Z. Xu and S. J. Bao, *Sens. Actuators, B*, 2022, **354**, 131201.

54 J. Deng, K. Wang, M. Wang, P. Yu and L. Mao, *J. Am. Chem. Soc.*, 2017, **139**, 5877–5882.

55 K. Lu, T. Aung, N. Guo, R. Weichselbaum and W. Lin, *Adv. Mater.*, 2018, **30**, 1707634.

56 L. He, M. Brasino, C. Mao, S. Cho, W. Park, A. P. Goodwin and J. N. Cha, *Small*, 2017, **13**, 1700504.

57 G.-B. Hu, C.-Y. Xiong, W.-B. Liang, X.-S. Zeng, H.-L. Xu, Y. Yang, L.-Y. Yao, R. Yuan and D.-R. Xiao, *ACS Appl. Mater. Interfaces*, 2018, **10**, 15913–15919.

58 W.-H. Chen, G.-F. Luo, Y. S. Sohn, R. Nechushtai and I. Willner, *Adv. Funct. Mater.*, 2019, **29**, 1805341.

59 Z. Wang, Y. Fu, Z. Kang, X. Liu, N. Chen, Q. Wang, Y. Tu, L. Wang, S. Song, D. Ling, H. Song, X. Kong and C. Fan, *J. Am. Chem. Soc.*, 2017, **139**, 15784–15791.

60 M. Sk, S. Banesh, V. Trivedi and S. Biswas, *Inorg. Chem.*, 2018, **57**, 14574–14581.

61 C. Hao, X. Wu, M. Sun, H. Zhang, A. Yuan, L. Xu, C. Xu and H. Kuang, *J. Am. Chem. Soc.*, 2019, **49**, 141.

62 Y. Liu, H. Wei, X. Jiang, H. Guo and X. Liu, *Electroanal. Chem.*, 2018, **820**, 51–59.

63 S. Dey, S. Maity, A. Dasmahapatra, D. Chattopadhyay and C. Sinha, *ChemistrySelect*, 2019, **4**, 4472–4477.

64 T. Fan, T. Xia, Q. Zhang, Y. Cui, Y. Yang and G. Qian, *Microporous Mesoporous Mater.*, 2018, **266**, 1–6.

65 Y. Li, X. Hu, X. Zhang, H. Cao and Y. Huang, *Anal. Chim. Acta*, 2018, **1024**, 145–152.

66 X. Shi, H. M. Meng, X. Geng, L. Qu and Z. Li, *ACS Sens.*, 2020, **5**, 3150–3157.

67 O. Troeppner, R. Lippert, T. E. Shubina, A. Zahl, N. Jux and I. Ivanovi'c-Burmazovi'c, *Angew. Chem., Int. Ed.*, 2014, **53**, 11452–11457.

68 P. Ravichandiran, A. Boguszewska-Czubara, M. Masłyk, A. P. Bella, S. A. Subramaniyan, P. M. Johnson, K. S. Shim, H. G. Kim and D. J. Yoo, *ACS Sustainable Chem. Eng.*, 2019, **20**, 17210–17219.

69 L. Notini, D. E. Latta, A. Neumann, C. I. Pearce, M. Sassi, A. T. N'Diaye, K. M. Rosso and M. M. Scherer, *Environ. Sci. Technol.*, 2018, **52**, 2751–2759.

70 Y. Lu, B. Yan and J. L. Liu, *Chem. Commun.*, 2014, **50**, 9969–9972.

71 Y. Kumar, R. Kaushik, S. Rani, S. Rafat, J. Shabir, K. Dev and L. S. Kumar, *Mater. Today Commun.*, 2021, **28**, 102563.

72 S. M. Hossain, V. Prakash, P. Mamidi, S. Chattopadhyay and A. K. Singh, *RSC Adv.*, 2020, **10**, 3646–3658.

73 Y. Zhang, Y. Li and L. Zhang, *Spectrochim. Acta, Part A*, 2021, **259**, 119892.

74 C. Szabo, C. Coletta, C. Chao, K. Modis, B. Szczesny, A. Pa-papetropoulos and M. R. Hellmich, *Proc. Natl. Acad. Sci. U. S. A.*, 2013, **110**, 12474–12479.

75 F. Yu, X. Han and L. Chen, *Chem. Commun.*, 2014, **50**, 12234–12249.

76 J. Liu, K. K. Yee, K. W. Lo, K. Y. Zhang, W. P. To, C. M. Che and Z. Xu, *J. Am. Chem. Soc.*, 2014, **136**, 2818–2824.

77 Y. Ma, S. Hao, X. Kuang, X. Li and T. Bo, *Anal. Chem.*, 2014, **86**, 11459–11463.

78 J. Wang, R. C. Zhang, Y. L. Cao, Y. A. Li, Y. R. Wang and Q. L. Wang, *New J. Chem.*, 2018, **42**, 3551–3559.

79 X. F. Yang, H. B. Zhu and M. Liu, *Inorg. Chim. Acta*, 2017, **466**, 410–416.

80 S. S. Nagarkar, T. Saha, A. V. Desai, P. Talukdar and S. K. Ghosh, *Sci. Rep.*, 2014, **4**, 7053.

81 X. Xin, J. Wang and C. Gong, *Sci. Rep.*, 2016, **6**, 21951.

82 A. Das, S. Banesh, V. Trivedi and S. Biswas, *Dalton Trans.*, 2018, **47**, 2690–2700.

83 A. Yuan, C. Hao, X. Wu, M. Sun, A. Qu, L. Xu, H. Kuang and C. Xu, *Adv. Mater.*, 2020, **32**, 1906580.1–1906580.7.

84 H. J. Forman, H. Zhang and A. Rinna, *Mol. Aspects Med.*, 2009, **30**, 1–12.

85 B. Ketterer, B. Coles and D. J. Meyer, *Environ. Health Perspect.*, 1983, **49**, 59–69.

86 E. Hatem, N. E. Banna and M. E. Huang, *Antioxid. Redox Signaling*, 2017, **27**, 1217–1234.

87 S. Awasthi, S. S. Singhal, R. Sharma, P. Zimniak and Y. C. Awasthi, *Int. J. Cancer*, 2003, **106**, 635–646.

88 K. Huang, L. Huang and R. B. Van Breemen, *Anal. Chem.*, 2015, **87**, 3646–3654.

89 W. Zhu, G. Jiang, L. Xu, B. Li, Q. Cai, H. Jiang and X. Zhou, *Anal. Chim. Acta*, 2015, **886**, 37–47.

90 P. Ni, Y. Sun, H. Dai, J. Hu, S. Jiang, Y. Wang and Z. Li, *Biosens. Bioelectron.*, 2015, **63**, 47–52.

This journal is © The Royal Society of Chemistry 2023

J. Mater. Chem. B, 2023, **11**, 6802–6822 | **6821**

91 J. Tang, B. Kong, Y. Wang, M. Xu, Y. Wang, H. Wu and G. Zheng, *Nano Lett.*, 2013, **13**, 5350–5354.

92 A. Saha and N. R. Jana, *Anal. Chem.*, 2013, **85**, 9221–9228.

93 J. H. Bong, H. W. Song, T. H. Kim, M. J. Kang, J. Jose and J. C. Pyun, *Biosens. Bioelectron.*, 2018, **102**, 600–609.

94 Y. Wang, K. Jiang, J. Zhu, L. Zhang and H. Lin, *Chem. Commun.*, 2015, **51**, 12748–12751.

95 Y. A. Li, C. W. Zhao and N. X. Zhu, *Chem. Commun.*, 2015, **51**, 17672–17675.

96 S. Zhu, S. Wang, M. Xia, B. Wang, Y. Huang, D. Zhang, X. Zhang and G. Wang, *ACS Appl. Mater. Interfaces*, 2019, **11**, 31693–31699.

97 P. Yang, Y. Zheng, Y. Wang, J. Yue, G. Gao, Y. Ma and B. Tang, *Sens. Actuators, B*, 2021, **348**, 130680.

98 H. Peng, A. M. Newbigging, M. S. Reid, J. S. Uppal and X. C. Le, *Anal. Chem.*, 2020, **92**, 292–308.

99 S. W. Kim, Z. Li, P. S. Moore, A. P. Monaghan and Y. Chang, *Nucleic Acids Res.*, 2010, **38**, 98.

100 C. Chen, D. A. Ridzon and A. J. Broomer, *Nucleic Acids Res.*, 2005, **33**, 179.

101 J. Q. Yin, R. C. Zhao and K. V. Morris, *Trends Biotechnol.*, 2008, **26**, 70–76.

102 Y. Wu, J. Han, P. Xue, R. Xu and Y. Kang, *Nanoscale*, 2015, **7**, 1753–1759.

103 X. Wei, L. Zheng, F. Luo, Z. Lin, L. Guo, B. Qiu and G. Chen, *J. Mater. Chem. B*, 2013, **1**, 1812–1817.

104 M. Hu, L. Zhu, Z. Li, C. Guo, M. Wang, C. Wang and M. Du, *Appl. Surf. Sci.*, 2021, **542**, 148586.

105 C. Yang, K. Wang, Z. Li, L. Mo and W. Lin, *Sens. Actuators, B*, 2022, **359**, 131593.

106 J. Xu, J. Guo, N. Golob-Schwarzl, J. Haybaeck, X. Qiu and N. Hildebrandt, *ACS Sens.*, 2020, **5**, 1768–1776.